



Universidad de Valladolid



**ESCUELA DE INGENIERÍAS
INDUSTRIALES**

UNIVERSIDAD DE VALLADOLID

ESCUELA DE INGENIERIAS INDUSTRIALES

Máster en Ingeniería Química

**A water-free route to porous materials via
cryoextraction and supercritical drying**

Autor:

Castedo Hernández, Cecilia

María José Cocero Alonso

Technische Universität Hamburg-Harburg

Valladolid, Abril 2021.

TFM REALIZADO EN PROGRAMA DE INTERCAMBIO

TÍTULO: A water-free route to porous materials via cryoextraction and supercritical drying

ALUMNO: Cecilia Castedo Hernández

FECHA: 26 de Marzo de 2021

CENTRO: Institute of Thermal Separation Processes (V8)

UNIVERSIDAD: Technische Universität Hamburg-Harburg

TUTOR: Jun.-Prof. Pavel Gurikov

Resumen

En el trabajo se ha desarrollado una nueva ruta, exenta de agua, para la preparación de materiales porosos a partir de polímeros que no pueden ser utilizados en la ruta convencional de producción de aerogeles. La nueva ruta está compuesta por cuatro etapas: disolución del polímero en DMSO, posteriormente congelación a -28°C , extracción del disolvente con etanol a baja temperaturas -28°C y secado supercrítico mediante CO_2 a 120 bar y 50°C .

Los materiales obtenidos se caracterizan mediante su superficie específica via medición BET y la contracción volumétrica. Entre todos los polímeros estudiados poliacrilonitrilo (PAN) es seleccionado para su estudio en profundidad. Materiales creados con PAN tienen una superficie específica de 119 y $107\text{ m}^2\text{g}^{-1}$ para concentraciones de 5 y 7,5 % en peso respectivamente. Su combinación con PVA y agar, así como la adición de urea provoca materiales de peores características, menor superficie específica y peores propiedades físicas.

Palabras clave

Aerogel, ruta de preparación, polímero, secado supercrítico, cryoextracción.

Hamburg University of Technology

Institute of Thermal Separation Processes

Master's Thesis

A water-free route to porous materials via cryoextraction and supercritical drying

by

Cecilia Castedo Hernández

Matriculation number: 497130

1st Examiner: Jun.-Prof. Dr. Pavel Gurikov
2nd Examiner: Prof. Dr.-Ing. Irina Smirnova
Supervisor: Jun.-Prof. Dr. Pavel Gurikov

05.10.2020 – 26.03.2021

Eidesstattliche Erklärung

Hiermit erkläre ich, Cecilia Castedo Hernández, geboren am 29.11.1996 in Spain, dass diese Diplomarbeit zur Vorlage beim Prüfungsamt der Technischen Universität Hamburg-Harburg von mir in selbständiger Arbeit, unter Verwendung der angegebenen Quellen angefertigt wurde.

Hamburg, den DATUM

Unterschrift

Einverständnis Erklärung

Ich gestatte der Technischen Universität Hamburg-Harburg die Diplomarbeit unter dem Gesichtspunkt des Urheberrechts für Zwecke in Forschung und Lehre nichtausschließlich und kostenfrei zu nutzen und zu vervielfältigen. Die Gestattung schließt die Weitergabe der Arbeit oder hiervon gefertigter Kopie zu wissenschaftlichen Zwecken an interessierte Dritte, die nicht der TUHH angehören müssen, ein.

Im Falle einer eigenen Verwertung der Diplomarbeit werde ich mich zuvor mit der TUHH in Verbindung setzen, damit diese die Arbeit zur Wahrung eventueller eigener Rechte und der Rechte ihrer sonst beteiligten Angehörigen (z.B. (Mit-) Erfindungsanteile des Betreuers oder anderer schutzrechtsfähiger Ergebnisse, die nicht oder nicht allein von mir stammen; Vermeidung der Weitergabe unrichtiger Ergebnisse unter Namensnennung der TUHH) prüfen kann.

Ich bin bereit, eigene patent- oder sonstige schutzrechtsfähige Erkenntnisse der TUHH auf Wunsch gegen Zahlung einer angemessenen Vergütung zu übertragen bzw. an mir erteilten Schutzrechten gegen Zahlung einer angemessenen Lizenzgebühr ausschließliche oder nichtausschließliche Nutzungsrechte einzuräumen.

Hamburg, den DATUM

Unterschrift

Abstract

In this study a novel process combining freezing, cryoextraction and supercritical drying for producing porous materials is developed. The process consists of three main steps: first of all, freezing a polymer/DMSO solution at $-28\text{ }^{\circ}\text{C}$ to obtain a monolith. Second step is solvent exchange with EtOH at $-28\text{ }^{\circ}\text{C}$ to extract DMSO crystals, obtaining an alcogel at the end of this process. The last part of the process is drying the alcogel with scCO_2 at 120 bar and $50\text{ }^{\circ}\text{C}$ for 3 h. The method has been used for the production of polyacrylonitrile (PAN) aerogels, it is demonstrated that for this material a high quality aerogel is obtained at 5 wt % volumetric shrinkage $36.8 \pm 6.1\%$, porosity is $93.5 \pm 0.6\%$ and $119 \pm 18\text{ m}^2\text{ g}^{-1}$ of specific surface area (SSA). In addition to PAN, other polymers such as poly(vinyl alcohol) (PVA) and agar-agar and their combination with PAN are tested. Pure PVA aerogels show the highest value of SSA at 7.5 wt % of $107 \pm 15\text{ m}^2\text{ g}^{-1}$. Both combinations result in a aerogel with worse quality than pure PAN. In particular, porosity and linear shrinkage experimented by PAN/PVA aerogels have a exponential relation with PVA concentration. In addition to standard conditions, liquid nitrogen at $-196\text{ }^{\circ}\text{C}$ is used as a freezing agent obtaining aerogels with lower SSA that lack physical integrity. However, whereas in conventional freezing at $-28\text{ }^{\circ}\text{C}$ directional freezing is observed, more pronounced with the decrease in concentration, for aerogels frozen at $-196\text{ }^{\circ}\text{C}$ non-hierarchical pore structures are found.

Generally speaking, it has been observed that lower concentrations leave more space for DMSO crystals to grow due to looser arrangement of polymer chains. At the same time, pore walls become thinner making the network weaker leading to higher shrinkage.

List of Symbols

Latin symbols

Symbol	Unit	Meaning
$V_{\text{shrinkage}}$	-	Volumen shrinkage
$l_{\text{shrinkage}}$	-	Linear shrinkage
SSA	m^2g^{-1}	Specific surface area
T_m	$^{\circ}\text{C}$	Melting point
T_b	$^{\circ}\text{C}$	Boiling point
T_{FR}	$^{\circ}\text{C}$	Process freezing temperature
V_{pore}	cc/g	Pore volume

Greek symbols

Symbol	Meaning
ε	Porosity
x_i	Molar fraction

List of Abbreviations

Abbreviation	Meaning
3D	Three dimensional
LMW	Low molecular weight
SEM	Scanning electron microscopy
BET	Braunauer-Emmett-Teller

Chemicals Abbreviations

Abbreviation	Chemicals name
scCO ₂	Supercritical carbon dioxide fluid
EtOH	Ethanol
MeOH	Methanol
Ac	Acetone
DMSO	Dimethyl sulfoxide
CMC Na Salt low	Carboxymethylcellulose sodium salt low viscosity
CMC Na Salt med	Carboxymethylcellulose sodium salt medium viscosity
PAN	Polyacrylonitrile
PVA	Poly(vinyl alcohol)

Content

1	Introduction and research purpose	1
1.1	Introduction	1
1.2	Research purposes	1
2	Fundamentals and State of the art	3
2.1	Polymeric gels	3
2.1.1	Properties of polymeric gels	4
2.1.2	Classification of polymeric gels	4
2.2	Gels classified by continuous phase	6
2.2.1	Hydrogels	7
2.2.2	Organogels	8
2.2.3	Xerogels	10
2.2.4	Aerogels	11
2.2.5	Cryogels	14
2.3	Examples for polymer gels	17
2.3.1	Polyacrylonitrile (PAN)	17
2.3.2	Poly(vinyl alcohol) (PVA)	18
2.3.3	Amide pectin	19
2.3.4	Carboxymethyl Cellulose Sodium salt	20
2.3.5	Inulin	20
2.3.6	Gum arabic	21
2.3.7	Agar-agar	22
2.4	Summary and Background of Study	23
2.4.1	Porous materials via cryoextraction	23

2.4.2	Screening of solvent and anti-solvent	27
2.4.3	Characterization of aerogels	29
3	Materials and methods	33
3.1	Materials	33
3.2	Preparation of aerogels	34
3.2.1	Dissolution of polymers	35
3.2.2	Cryoextraction with ethanol	35
3.2.3	Supercritical CO ₂ drying	36
3.3	Screening of process variables	38
3.3.1	Solubility of polymers in DMSO and TBA	38
3.3.2	Freezing moulds	38
3.3.3	Thickness of monolith	39
3.3.4	Freezing temperature	40
3.4	Characterization of aerogels	40
3.4.1	BET adsorption isotherm	40
3.4.2	Scanning electron microscopy	42
4	Results and discussion	43
4.1	Different polymers	43
4.1.1	Solubility	43
4.1.2	Cryoextraction	44
4.1.3	Properties of the gels	44
4.2	PAN aerogels	46
4.2.1	Effects of the freezing mould	52
4.2.2	Thickness of the monolith	56
4.2.3	Effect of freezing temperature	58
4.3	PAN based aerogels	62

4.3.1	PAN/urea aerogels	63
4.3.2	PAN/PVA aerogels	64
4.3.3	PAN/agar-agar aerogels	68
5	Summary	71
6	Conclusions and outlook	74
7	Appendix	76
7.1	Calibration curves of EtOH and solvent mixtures	76
	Literature	78

List of Figures

Figure 2.1:	Simplified percolation model for sol phase and gel phase, reprinted from [12].	4
Figure 2.2:	Schematic representation of (a) a physical gel formed by association of macromolecular chains and (b) a chemical gel formed through polymerization and crosslinking reaction, reprinted from [18].	6
Figure 2.3:	Classification of hydrogels based on the different properties.	7
Figure 2.4:	General classification of organogels [28].	9
Figure 2.5:	Pristine silica aerogel monolith with schematic structural build up, reprinted from [35].	12
Figure 2.6:	Scheme of formation of macroporous gels, reprinted from [41].	15
Figure 2.7:	A schematic representation of a binary phase diagram of a polymer solution showing a liquid-liquid demixing gap, reprinted from [44].	16
Figure 2.8:	Molecular structure of PAN, reprinted from [49].	18
Figure 2.9:	Molecular structure of PVA, reprinted from [61].	19
Figure 2.10:	Molecular structure of pectin and amidated pectin with ethanolamine, reprinted from [66].	19
Figure 2.11:	Molecular structure of CMC sodium salt, reprinted from [71].	20
Figure 2.12:	Molecular structure of inulin, reprinted from [71].	21
Figure 2.13:	Molecular structure of agar-agar, reprinted from [80].	22

Figure 2.14:	SEM images of the pore structure of the material. a) Lateral view of 10 wt% PVA. Freezing direction highlighted with a red arrow. b) Axial view. Reprinted from [96].	26
Figure 2.15:	SEM images of (a) APPF-3, (b) APPF-5, (c) APPF-7, and (d) APPF-9 at the transverse cross-section (green dashed lines represent the pores in APPFs). (e) Pore size distribution of APPF-3, APPF-5, APPF-7, and APPF-9 as measured by Hg intrusion porosimetry. (f) Average thickness of the wall adjacent to the pores and the bulk density of APPFs vs PAN concentration. Reprinted from [97].	27
Figure 2.16:	Molecular structure of DMSO.	28
Figure 2.17:	Curve (A) adsorption isotherms of nitrogen at 77 K on non-porous silicas and aluminas. Curve (B) adsorption isotherm calculated from equation. Reprinted from [109].	31
Figure 3.1:	Preparation route for PAN aerogels.	34
Figure 3.2:	250 ml autoclave for scCO ₂ drying.	36
Figure 3.3:	Moulds tested for the preparation of aerogels: (a) Candle mould before preconditioning (b) Candle mould (c) Hard mould (d) Aluminium plate (f) Plastic syringe.	39
Figure 3.4:	Cell culture plate size 6 wells.	39
Figure 3.5:	Surface area and pore size analyzer NOVA 4000e.	41
Figure 4.1:	Comparison of specific surface area. ■ solvent DMSO ■ solvent TBA and ● porosity. Individual concentration is expressed in the correspondent bar.	46
Figure 4.2:	PAN aerogel properties at different concentrations.	48

Figure 4.3:	Comparison of linear shrinkage in solvent exchange and scCO ₂ drying of PAN aerogels, ■ scCO ₂ drying ■ EtOH exchange. . .	49
Figure 4.4:	PAN aerogel 7.5 wt% with radial heterogeneity. (a) After solvent exchange (b) after supercritical drying.	50
Figure 4.5:	PAN aerogel 5 wt%.	51
Figure 4.6:	SEM images of PAN 2.5 wt% aerogel.	51
Figure 4.7:	SEM images of PAN 5 wt% aerogel.	53
Figure 4.8:	PAN aerogel in syringe: (a) 0.625 wt% (b) 5 wt%.	54
Figure 4.9:	Comparison of specific surface area, density and volumetric shrinkage for different moulds.	55
Figure 4.10:	Comparison of specific surface area, porosity and volumetric shrinkage for different grams ■ 5g ■ 10g.	57
Figure 4.11:	Comparison of specific surface area, porosity and volumetric shrinkage of PAN aerogels different freezing temperature ■ -28 °C ■ -196 °C.	60
Figure 4.12:	SEM images of PAN 5 wt% aerogel frozen at -196 °C.	62
Figure 4.13:	Comparison of specific surface area, porosity and volumetric shrinkage of PAN aerogels ■ 5 wt% ■ 7.5 wt% with the concentration of urea.	64
Figure 4.14:	Comparison of specific surface area, density and volumetric shrinkage for ■ PAN and ■ PVA.	66
Figure 4.15:	Effect of ratio PAN/PVA of aerogels 5 wt % on specific surface area, porosity and linear shrinkage.	68
Figure 4.16:	PAN/Agar-agar(50/50%) 7.5 wt% aerogel (a) top side (b) bottom side.	69

Figure 4.17:	Comparison of specific surface area, porosity and volumetric shrinkage of aerogels ■ PAN ■ hybrid PAN/Agar (50/50%). .	70
--------------	--	----

List of Tables

Table 2.1:	Solvents in which polymers are soluble	28
Table 3.1:	List of chemicals used in this study.	33
Table 4.1:	Polymers soluble in DMSO and TBA/Water.	44
Table 4.2:	Results of properties of different polymers' aerogels.	45
Table 4.3:	PAN aerogel properties at different concentrations.	47
Table 4.4:	Results of PAN aerogels in different moulds.	56
Table 4.5:	Results of PAN aerogels with change is sample size.	58
Table 4.6:	Results of PAN aerogels frozen with liquid nitrogen.	59
Table 4.7:	Results of properties of hybrid PAN/urea aerogels at different compositions.	63
Table 4.8:	Results of properties of pure PAN and PVA aerogels at different compositions.	65
Table 4.9:	Results of properties of hybrid PAN/PVA aerogels at different ratios at concentration 5 wt%.	67
Table 4.10:	Results of properties of pure PAN and hybrid 50% PAN 50% agar-agar aerogels at different polymer concentration.	69
Table 7.1:	Skeletal densities of polymers.	76
Table 7.2:	Density of mixtures of EtOH and DMSO. Calibration data. . .	77
Table 7.3:	Density of mixtures of EtOH and DMSO aqueous solution of TBA at 20% density. Calibration data.	77

1. Introduction and research purpose

1.1 Introduction

Gels are semisolid materials made at least of two constituents, that possess elastic characteristics. The constituents are usually a polymer and solvent, the polymer forms a 3D network structure able to trap the solvent. Gels are characterised for their limited swelling degree. Polymer gels are observed in human bodies, the cornea, vitreous and connective tissues [1, 2, 3].

Gels can be classified in different types of gels based on different properties. Among all of them, aerogels are known to be a highly porous material, with low density $0.003\text{--}0.15\text{ kg m}^{-3}$ and relatively high specific surface area $300\text{--}1500\text{ m}^2\text{ g}^{-1}$. These unique properties make aerogels exceptional materials for a wide range of applications such as insulating materials, catalysts, thickening agents, water repellents, gas filters [4, 5]. Currently research has been done focused on different biopolymer aerogels for their potential use in the biomedical industry such as cardiovascular implantable devices, tissue engineering substrates, drug delivery systems [5, 6].

1.2 Research purposes

Production of aerogels with the conventional route have some limitations related to the material's nature and the use of water as a solvent. For example, some materials are complicated and in some cases impossible to turn into a wet network in the gelation step. When water is used as a solvent it is required a solvent exchange

step with an antisolvent compatible with CO₂ at supercritical conditions to assure minimal collapse of the network. As a result, binary mixture of EtOH and water is formed which has a azeotrope at 96%, thus, recycling of the mixture is very complex[7]. The aim of this work is to further study the route established by Ching Ma [8] that overcomes these limitations for different polymers and optimization of process parameters.

2. Fundamentals and State of the art

In this chapter the current research and fundamentals of polymer gels and specific polymers are presented. Afterwards the current state of the art is discussed.

2.1 Polymeric gels

Polymeric gels are defined as soft and/or solid-like systems made of one polymer or more than one polymer [9]. These systems usually consist of the polymer and the solvent, the interaction with each other create a three-dimensional (3D) network able to trap a solvent [10]. A wide variety of polymers, such as gelatins, collagen, alginates, polysaccharides, cellulose are available in the nature [11]. Their properties, biodegradability and biodiversity, make these systems have multiple applications. For these reason, in the past years, they have gained interest among researchers around the world [3].

The mechanism by which polymeric gels are form can be described by the percolation model. In this model, chemical bonds between monomeric subunits are created randomly in order to create independent clusters. The continuous paths in which they grow result in a discontinuous change of the system properties [12]. When a certain amount of bond is reached, the individual agglomerates bond into a single agglomerate, Figure 2.1, and the system changes from sol to gel.

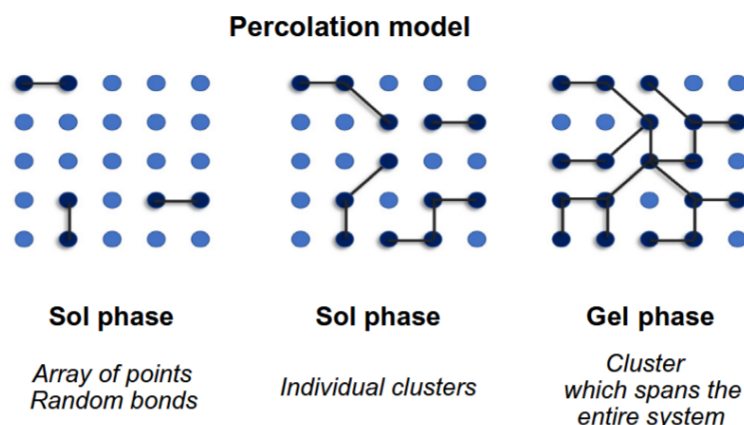


Figure 2.1: Simplified percolation model for sol phase and gel phase, reprinted from [12].

2.1.1 Properties of polymeric gels

Depending on different factors, such as polymers, nature of cross-linking, size, polymeric matrix types, polymeric gels have a different set of properties. One of the important properties is swelling, the capacity of the solvent molecules to be absorbed and confined in the polymer network. During this process gel-gel interactions are restored via the gel-solvent interactions [13].

2.1.2 Classification of polymeric gels

Classification of polymer gels can be made based on different characteristics (solvent in the 3D network, polymers that form the gel and formation method of polymer network). In this case, the classification will be by the nature of the chemical linkage.

Polymeric gels can be classified into three different categories, physical, chemical and entanglement network gels [13].

Physical gels are formed by the aggregation caused by hydrophobic, electrostatic,

van der Waals or hydrogen bond interactions. The cross-linking of these gels is temporary which causes some gels to be thermoreversible being able to be liquefied or dissolved, some conditions that influence this instability are temperature, pH and ionic strength. This behaviour depends in every physical gel based on the material types and characters [3]. One example is aqueous solutions of agar and gelatin that become gels if the temperature is lowered and it will become solution again if the temperature is increased [14]. Different methods for the cross-linking are: hydrogen bonding, ionic bonding, coordination bonding, helix formation, hydrophobic bonding [14].

Physical gels can be further classified into "strong" physical gels and "weak" physical gels [15]. The difference between these two is that strong gels are solid in the large deformations and weak gels are structured fluids and flow as the liquid at larger deformations [16].

Chemical gels (also known as covalently cross-linked gels) are prepared through different methods, for example: addition polymerization of oligomeric multi-functional precursors, vulcanization of high-molecular weight linear polymeric chains, end linking of the reactive chains with branching units, etc [16]. Due to the nature of network's junctions, covalent bonding between the macromolecules and the cross-linkers, these gels can only be damaged via de bond rupturing or by thermal degradation of polymer [17]. Due to their covalent bonding they have a permanent structure for swelling and shrinking in a dynamic reversible way and are less susceptible to external variables [12]. Contrary to physical gels, they generally do not dissolve.

The difference between physical and chemical gels is shown in Figure 2.2

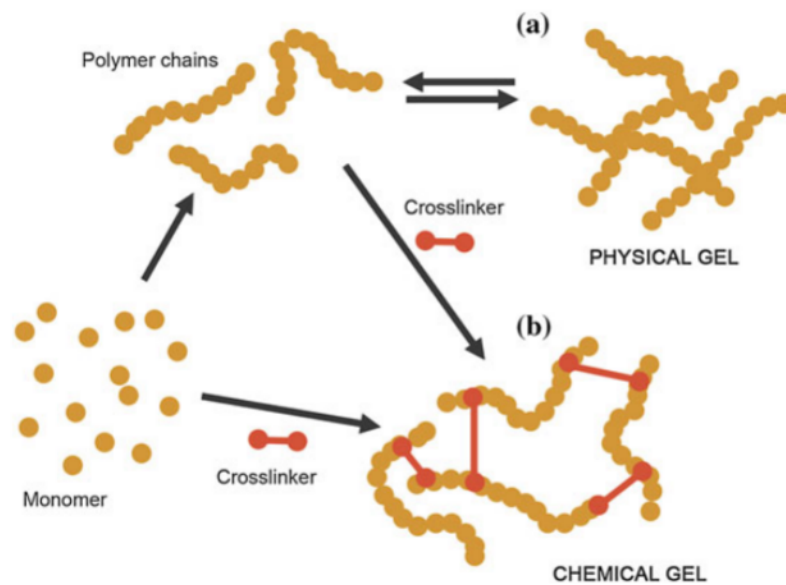


Figure 2.2: Schematic representation of (a) a physical gel formed by association of macromolecular chains and (b) a chemical gel formed through polymerization and crosslinking reaction, reprinted from [18].

Entanglement networks are formed via topological interactions of polymeric chains either in the melt or in the solutions, when the concentration and molecular weight of the entanglement network is higher than the critical molecular mass for the entanglement [16]. This behaviour is observed in polymeric gels that contain polymer(s) of high molecular weight, specially elastomers. These gels are usually dissolved in a suitable solvent to produce dilute polymer solutions [16].

2.2 Gels classified by continuous phase

According to the definition of gels there are multiple examples of them. Gels that are explained on the following pages could present different classification depending on the properties mentioned in section 2.1.2.

2.2.1 Hydrogels

Hydrogels are three-dimensional cross-linked polymer networks which can absorb and retain large amount of water [19], mostly made of hydrophilic polymer(s) [20].

The classification of hydrogels, Figure 2.3 [21, 22, 23]:

- Based on source: Natural, synthetic or hybrid.
- Based on the preparation method: Homopolymeric hydrogels derived from only one specie of monomer, copolymeric hydrogels with tho or more different monomers and multipolymer interpenetrating polymeric hydrogel (IPN) made out of two independent polymers that are in a network form.
- Based on configuration: Amorphous, semicrystalline and crystalline.
- Based on the type of cross-linking (see Section 2.1.2): chemical or physical hydrogels.
- Based on physical appearance: It is influenced by the production process and they can be matrix, microspheres and films.
- According to network electrical charge: nonionic, cationic and anionic.
- Based on their response to chemical, biochemical or physical stimuli.

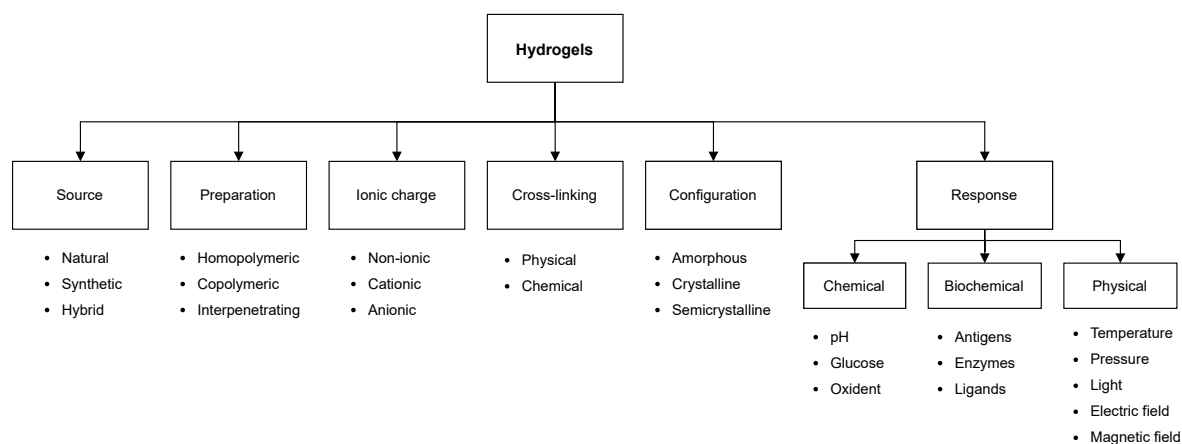


Figure 2.3: Classification of hydrogels based on the different properties.

The capability of hydrogels for absorbing fluids arises because of the hydrophilic functional groups of the constituent polymeric backbone. This swelling behaviour of hydrogels depend on the environmental conditions, such as pH, temperature, ionic strength, and electromagnetic radiation [24]. Not only that property is dependant of those conditions but also, shape, mechanical flexibility, opacity, and porosity can be modified [25]. These multifunctional properties make hydrogels a very attractive material for their application in a variety of fields, such as biomedical science, drug delivery, water purification, tissue engineering, agriculture and sensor [26].

Hydrogels can be obtained from different natural or synthetic material. Some natural polymers that can be used to produce hydrogels are collagen, gelatin, fibrin, hyaluronic acid, heparin, alginates, pectins, chitosan [27]. Hydrogels can be produced by reactive cross-linkers, copolymerization, or free-radical polymerization. This material can be obtained in a number of ways including ionization, linking polymer in a chemical reaction, or physical interactions [25].

Multiple methods can be use for the synthesis of physical and chemical hydrogels. For physical hydrogels the important methods are hydrogen-bonding interaction, hydrophobic interaction, ionotropic interaction, stereo-complexation, inclusion complexation.

2.2.2 Organogels

Organogels are defined as semi-solid systems comprised of gelator molecules (concentration lower than 15 wt %) and an organic solvent forming a 3D network through molecular interaction [28]. For this reason, organogels are considered bicontinuous

systems that may or may not restrain aqueous molecules trapped within the different self-assembled structures of gelators [3].

Organogels can be divided according to different criteria, e.g. based on the nature of the gelling agent: polymeric or low molecular weight (LMW) organogelators [29], the type of interaction between molecules, based on organogel properties, solvent used and preparation model [30]. Depending on the network that is created, polymeric gelators can be further classified into physical or chemical gels, section 2.1.2. LMW organogels only form physical gels, they create aggregate capable of immobilizing the solvent. Furthermore, based on the type of organogel they can be classified in solid (strong) or fluid (weak) fiber networks [28]. The classification of organogels can be seen in Figure 2.4. Common gelators used for the preparation of organogels are lecithin, cholesteryl anthraquinone derivatives, sterol, sorbitan monoesterate, etc. Polymers immobilize the organic solvent by forming a network of either cross-linked or entangled for chemical and physical gels [29].

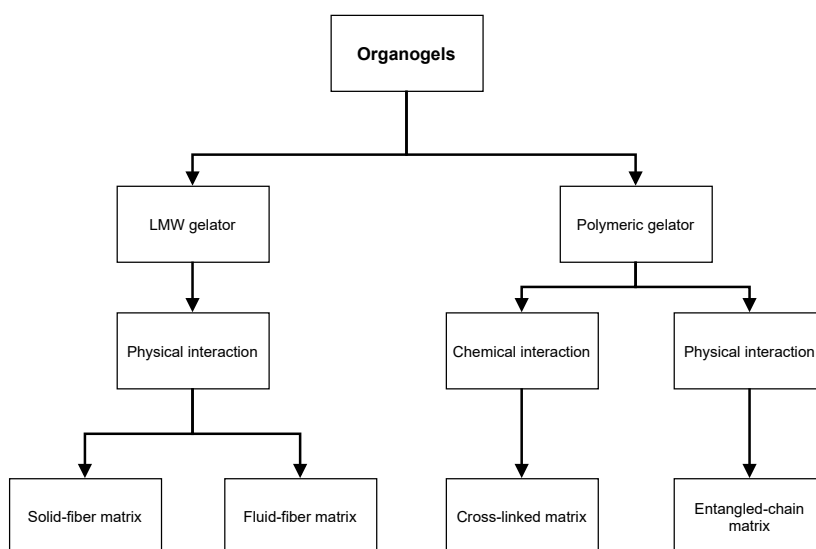


Figure 2.4: General classification of organogels [28].

Main properties possessed by organogels are thermostability, thermoreversibility,

optical clarity, viscoelasticity, etc. They are thermodynamically stable due to the spontaneous formation of fibrous structure by virtue of which the organogels reside in a low energy state [31].

Their application have a wide range in different fields such as paint and cleaning supplies, dermocosmetics and personal care products, nutraceuticals and food processing [30]. In addition, due to their entangled fibrous nano/microstructure, their use as a system in drug delivery applications has been studied. In the recent years, there has been advances in the formulation of biocompatible organogels that could be used as clinical products [30].

2.2.3 Xerogels

Xerogels are solid-formed gels dried by evaporation at elevated temperatures and ambient pressure. These conditions produce capillary pressure that lead to uncontrolled shrinkage [32]. Generally, xerogels have high porosity and large surface area ($100\text{--}1000\text{ m}^2\text{ g}^{-1}$) together with small pore size ($\leq 2\text{--}5\text{ nm}$) [33]. The method for preparation of xerogels is via the sol-gel mechanism in which metal alcoxide precursor, water and ethyl alcohol are used [3]. Applications of xerogels vary based on their porosity, for example, xerogel dense films are used as coating materials to avoid corrosion and films and porous films are used as membranes [33]. They are also used as fillers for polymer matrixes because of their already mentioned properties. Guzel Kaya *et al.* [34] proved that epoxy matrix filled with silica xerogels enhanced the thermal and acoustic performance of the material.

2.2.4 Aerogels

Aerogels are generally sol–gel materials that have gas as their continuous phase, by volume, 90–99 wt % of the material is air or gas [3]. Consequently their density range between 0.003–0.15 kg/m³. Because of the high porosity open micro and mesopores, they have a very high specific surface area (300–1500 m² g⁻¹) [35]. Their characteristic properties, low density, high specific surface area and high porosity, as well as the flexibility to control these properties by changing parameters of the process, make aerogels and their applications very promising. However, their use on a large scale is limited at this moment [35]. Some of the applications are thermal insulation, removal of pollutants and biomedical applications.

Aerogels can be classified based on their material application, porous structure and their composition [36].

- Based on the application can be monolith, powder or film forms.
- Based on the porous structure can be classified as microporous, mesoporous and mixed porous.
- Based on the composition they can be: inorganic, organic or hybrid.

2.2.4.1 Preparation of aerogels

These materials are synthesized by the following steps [3]:

1. Sol–gel transition (i.e., gelation): Sol particles are assembled and cross-linked into a wet–gel spontaneously or catalyzed via hydrolysis or condensation reactions.
2. Network perfection (i.e., aging): Mechanically reinforce the weak solid struc-

tures produced in the previous step.

3. Gel–aerogel transition (i.e., drying): The solvent is replaced by air without damaging the microstructure.

All of these steps determine the final microstructure and characteristics of the aerogel. The microstructure of aerogels is formed by a solid continuous network of primary and secondary colloidal particles connected to each other either by condensation or cross-linking or by the formation and aggregation of fibrils due to the rearrangement of polymer chains or macromolecules, Figure 2.5.

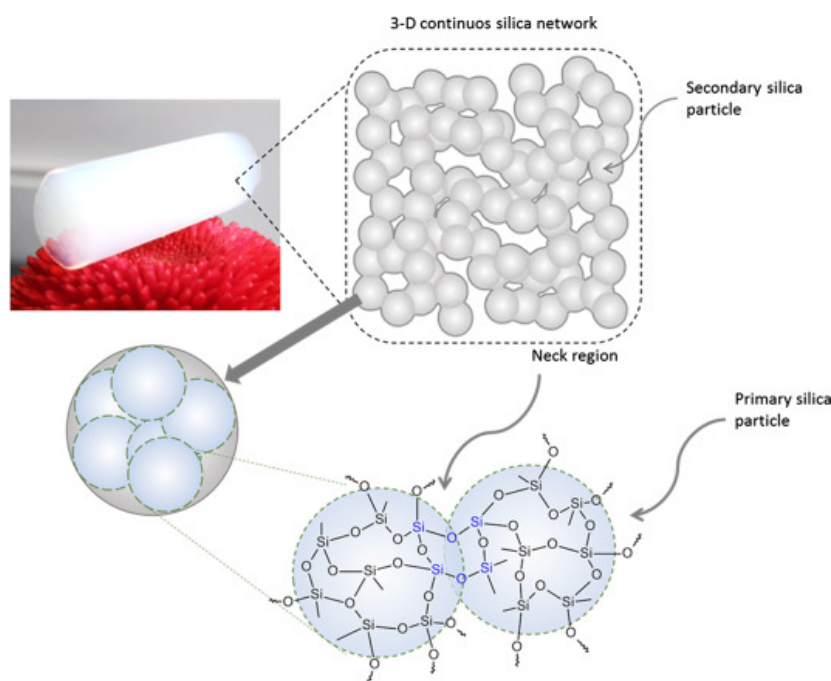


Figure 2.5: Pristine silica aerogel monolith with schematic structural build up, reprinted from [35].

Drying is a very important step in the preparation of aerogels. The microstructure of the aerogel should be almost identical to the one of the wet gel. The main problem is that during this process the wet gel could suffer a considerable shrinkage due to capillary forces. This capillary forces are the result of a large solid-liquid interface generated by the diameter (2–50 nm) of the mesopores contained in the aerogel. This

interfacial capillary forces lead to high capillary pressure gradient which causes the pores to pull on themselves and the consecutive reaction between molecules [35].

Some of the techniques are ambient drying, freeze drying and supercritical drying. Among these techniques supercritical drying is the classical drying method. This method avoids the existence of any intermediate vapor-liquid transition cancelling capillary forces and consequently, the collapse of the structure. This is done by pressurizing and heating the solvent beyond its critical point being a single supercritical fluid phase [37]. At the critical point the surface tension is zero and the fluid does not create any forces on the gel structure [32].

Supercritical carbon dioxide (scCO₂) is commonly used as a solvent to dry aerogels, due to its relative low critical pressure (72.8 bar) and critical temperature (30.95 °C). This characteristic allows it to replace any other organic miscible solvent inside of the pores, like ethanol or acetone.

2.2.4.2 Solvents during drying process

During the scCO₂ drying process, as a liquid mixture is formed between CO₂ and the solvent inside of the pores of the wet gel, it is important for the process to avoid any liquid-vapor transition. To achieve this, properties of the mixture CO₂-solvent at critical conditions have to be studied.

Consequently, it is important to have a solvent that has the proper characteristics in its supercritical mixture with CO₂ in order to have optimal drying conditions. This condition is not fulfilled by every solvent used for the dissolution of the substrates, therefore, solvent exchange has to be done before the drying. Solvents used for the exchange must be miscible with CO₂ and commonly methanol (MeOH), ethanol

(EtOH), acetone (Ac), dimethyl sulfoxide (DMSO), ethylene glycol, 2-propanol are used. Among these solvents ethanol is preferred due to its low vapour pressure and non-toxicity [38]. Multistep solvent exchange with EtOH increasing the concentration of the solvent each step results in lower shrinkage [39]. Not only solvents have to be miscible with CO₂ but must have a small miscibility gap in order to operate at reasonable mild conditions to preserve aerogel backbone. Gurikov *et al.* [7] studied the effect of different anti-solvents in shrinkage during solvent exchange and scCO₂ drying for alginate and guar galactomannan gels. One significant result shows that solubility parameters and hydrogen bonds expressed with the Hansen solubility parameters, have a relation with shrinkage.

In conclusion, the selection of the solvent is a crucial step and has to be done carefully taking into account different factors: miscibility of solvent with scCO₂ and properties of the solvent that could have an impact in the final aerogel, i.e. toxicity of solvent residuals.

2.2.5 Cryogels

Cryogels have gained a lot of attention in the last years in the medical fields for their potential application as tissue scaffolds. The term 'cryogel' comes from 'cryo' that means cold or ice and the already mentioned 'gel'. The scientific definition for these gels is not fixed, so multiple definitions are used to three different groups of substances [40]: (1) gelatinous precipitate formed during cryoprecipitation - blood plasma treatment upon cooling at 4 °C; (2) polymeric gels produced by the sol-gel method followed by freeze drying; (3) synthetic and natural polymers produced in a frozen solvent, usually water. In this process ice crystals are formed and used as a

porogen, and removed by thawing instead of freeze-drying.

Contrary to conventional gels, cryogels are heterophase systems where the solvent is inside the pores and bound to the polymer network [41]. These pores have a size of 1–100 μm and they are surrounded by thin walls of a highly concentrated polymer. The route followed for their preparation is shown in Figure 2.6. Preparation of porous material via thermally induced phase separation (TIPS) has been studied for the preparation of membranes [42, 43]. This method is based on the phenomenon that the solvent quality usually decreases when the temperature is decreased. After demixing is induced, the solvent is removed by extraction, evaporation or freeze drying [44]. Transition from polymer solution to porous structure has an important role in the final properties of the material. In the phase diagram of a binary polymer system three regions can be distinguished inside of the binodal curve determined by the spinodal curve, Figure 2.7. Depending on the concentration, liquid-liquid demixing proceeds through different mechanism. Inside the region located between the binodal and spinodal metastable compositions are obtained. Only processes with the same concentration as the critical point or processes with high freezing rate avoid demixing in the metastable region [45].

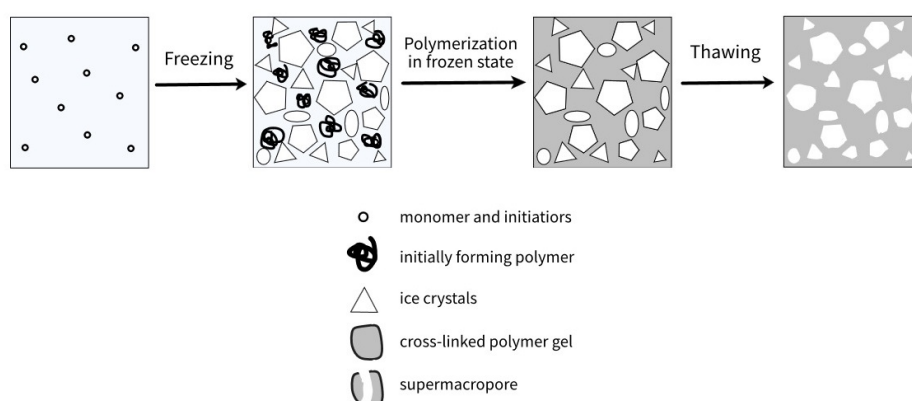


Figure 2.6: Scheme of formation of macroporous gels, reprinted from [41].

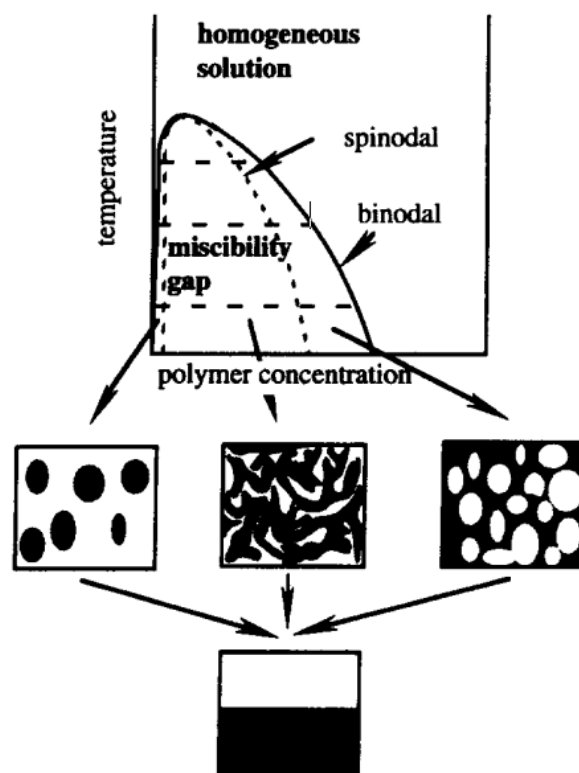


Figure 2.7: A schematic representation of a binary phase diagram of a polymer solution showing a liquid-liquid demixing gap, reprinted from [44].

These gels can be made with any monomer that could be polymerized by radical polymerization in aqueous solution. Pore size can be controlled with the temperature and also the nature and concentration of the monomer. Temperature has an effect in the final structure and the reaction rate. Lower temperature produces more ice nucleation sites but smaller, faster freezing and smaller non-liquid phase. If temperature is lower than the system's eutectic point, cryogels cannot be formed as no liquid phase is present [40].

2.3 Examples for polymer gels

Polymer and biopolymer aerogels have gained a lot of interest in the past years, approximately 17.8% of the literature studies. These polymer aerogels present very attractive applications and properties in different fields such as energy and biomedicine [46]. Production of hybrid aerogels from synthetic and natural based polymers have been studied [47]. Production of aerogels derived from synthetic polymer has mainly be done for polyureas, polyurethanes, polynorbornene, polydicyclopentadiene all of them in a monolithic shape [48].

Following there is a brief explanation of various polymers with current research on gel formation and their potential applications.

2.3.1 Polyacrylonitrile (PAN)

Polyacrylonitrile (PAN) is a derivative of polyethylene that has a nitrile (CN) group in the unit structure, Figure 2.8 [49], widely prepared by using nitrle polymerization [50]. It has strong intermolecular bonds, resulting in good barrier properties [51]. PAN has high thermal stability i.e, a high melting point. It is difficult to melt due to the cyclization of the nitrile group. It also shows high mechanical strength, dielectric constant and high dipole moment (3.9D) that causes strong polarity. Hence, it is capable to form stable fibers and nanofibers by electrospinning, spin casting, gel spinning, and dry-jet wet spinning [52].

Research on gel materials that contain PAN has been made over the past years for a wide variety of applications in different fields. For example, in the develop of smart materials Umemoto *et al.* [53] produced pH-sensitive hydrogel fibres from polyac-

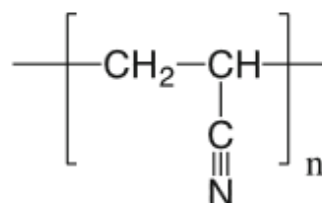


Figure 2.8: Molecular structure of PAN, reprinted from [49].

rylonitrile (PAN) textile fibers; in the medical field Ramseyer *et al.* [54] developed an injectable PAN-based hydrogel powder for the treatment of urinary incontinence; Mao *et al.* [55] developed the solvent-sensitive artificial muscle by hydrolyzed acrylonitrile-g-cellulose fiber; Yu *et al.* [56] studied the pH response of hydrolyzed PAN-blen-gelatin hydrogel fibers. Some authors have developed material for bone tissue engineering with electrospinning of PAN [57, 58]. Bhuiyan *et al.* [59] developed a PAN-silica aerogel nanofibre fabric with resistance against radiant heat and liquid penetration.

2.3.2 Poly(vinyl alcohol) (PVA)

Poly(vinyl alcohol) (PVA) is a simple hydrophilic biodegradable polymer containing a single hydroxyl group per monomer polymerized, Figure 2.9 from vinyl acetate followed by hydrolysis. PVA is commonly used as a hydrogel or as a sponge and can be chemically cross-linked using small-molecule bifunctional cross-linking agents like glutaraldehyde or through gamma irradiation or can undergo repeating freeze/thaw cycles to form physical cross-links between polymer chains [60].

PVA has a unique combination of properties such as solubility in water, film orientation characteristics for the polarizer of a liquid crystal display, adhesive ability to a number of substrates, low toxicity, biodegradability and biocompatibility. These

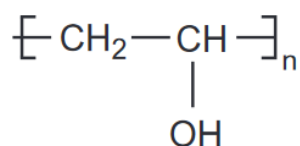


Figure 2.9: Molecular structure of PVA, reprinted from [61].

properties make PVA a very interesting material in chemical, material and biomedical fields [62].

2.3.3 Amide pectin

Pectins are structural polysaccharides of vegetable origin. The polymer backbone is based on (1→4)-linked α -D-galacturonate residues interrupted by insertion of (1→2)-linked rhamnosyl residues where the neutral sugar side chains are attached [63]. Pectin has been used as gelling agent, stabilizers, emulsifiers, and bioactive components in the food, pharmaceutical and cosmetic industry. However one negative property that impacts in their use is that it tends to form lumps when it is dispersed in water [64]. One of the solutions for this problem is to enhance the functional attributes of pectin by the amidation of pectin. The amidation is obtained by the action of ammonia on the ester groups of pectin under alkaline conditions [65].

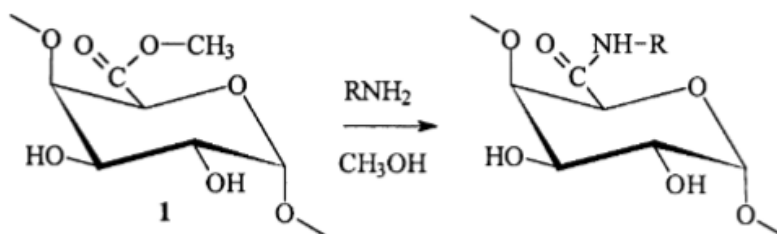


Figure 2.10: Molecular structure of pectin and amidated pectin with ethanolamine, reprinted from [66].

2.3.4 Carboxymethyl Cellulose Sodium salt

Carboxymethyl cellulose (CMC) is cellulose ether made by reaction of alkali cellulose with an alkyl halide [67], Figure 2.11. It is produced by treatment of cellulose with aqueous sodium hydroxide solution and subsequent reaction with monochloroacetic acid or its sodium salt [68]. Purified CMC is a white to off-white, non-toxic, odorless, biodegradable powder, which can be dissolved in hot or cold water [69]. CMC is used in numerous industries, cosmetic and pharmaceutical, textile, paper, ceramic, and food industry [70].

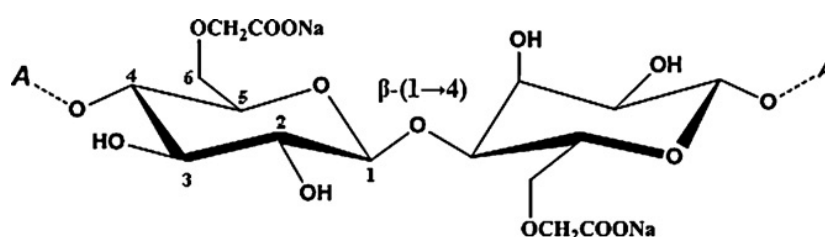


Figure 2.11: Molecular structure of CMC sodium salt, reprinted from [71].

2.3.5 Inulin

Inulin is a non-starch polysaccharide and can be found in a large number of plants such as chicory, Jerusalem artichoke, onion, garlic, barley, rye [72]. It is composed of β-D-fructofuranosyl units linked 2→1.

Some properties of inulin are, solubility in water at 40–80 °C with a concentration lower than 50%. Thermoreversible gels are formed when the concentration is higher than 25% and there is a cooling of the solution. The rheological properties of inulin gels make their use as a fat replacer in the food industry very common [73]. In addition to its rheological properties, there are studies that show their health benefits

and their food application fibre enrichment, as a prebiotic and as a sugar replacer [74]. They are also used in feed and pet food [75].

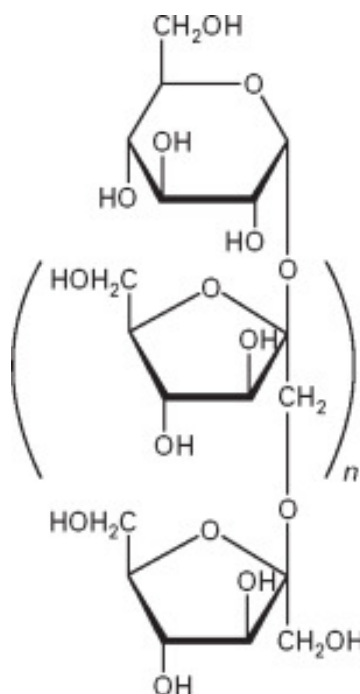


Figure 2.12: Molecular structure of inulin, reprinted from [71].

2.3.6 Gum arabic

It is a tree gum exudate that it is called also *Acacia* gum, there are two species of acacias that the regulation acknowledge as the trees for the extraction gum, *Acacia senegal* and *Acacia seyal*. Both gums consist of polysaccharides and contain a small amount of nitrogenous material that cannot be removed. The difference between the two gums is that *A. seyal* gum has lower rhamnose, glucuronic acid content and lower proportion of nitrogenous material [76].

Gum arabic is a highly heterogeneous material that consists of highly branched polysaccharides species. It can be divided into three fraction, a 70%–90% polysaccharide molecules, 10% of high molecular weight molecules that have a hydro-

phobic protein which provides the functionality of the gum, and the last fraction only up to 1% is a glycoprotein [77].

Gum arabic is mainly used in the food industry in different applications, in confections to reduce or prevent sucrose crystallization and to avoid the accumulation of fatty components on the surface. It is also used in beverages, bakery and dairy. Not only its uses are limited to food industry but to the textile, ceramics and pharmaceutical industry [78]. It is used as a suspending agent, emulsifier, adhesive and binder.

2.3.7 Agar-agar

Agar is a polymer composed of two fractions: neutral agarose and anionic agaropectin. It is a linear chain of 3-O-substituted β -D-galactopyranosyl units joined by (1 \rightarrow 4) linkages to 3,6-anhydro- α -L-galactopyranosyl units, its molecular structure can be seen in Figure 2.13. They are extracts from agarophyte members of the Rhodophyta. The pattern of substituting groups depends on the species, environmental factors and physiological [79].

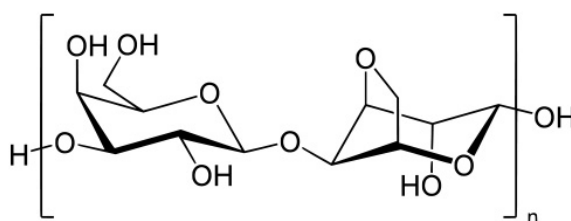


Figure 2.13: Molecular structure of agar-agar, reprinted from [80].

Agar is soluble in boiling water but insoluble at lower temperature, it forms gels at 30–40 °C. Gelation mechanism is based on the aggregation of helices and subsequent phase separation. Properties of the gel depend on agarose content degree

of sulfonation, generally with higher content and lower degree better and stronger gels are formed [81].

Applications of agar based in the gelling power, high hysteresis and perfect gel reversibility. Mainly it is used in the food industry and for biotechnological applications [82]. Research has been conducted in the field of aerogel production [83, 84, 85].

2.4 Summary and Background of Study

2.4.1 Porous materials via cryoextraction

As mentioned in section 2.3, biopolymer aerogels have gained a lot of interest in the past years, these aerogels are mainly prepared with the routed explained in section 2.2.4.1. Therefore, a gel from an aqueous solution must be created in the first step. Cardea *et al.* [86] successfully developed a production path for chitosan aerogels that combines cryogels and aerogels, in which there is a step of solvent exchange and low temperatures followed by scCO₂ drying. The formation of the polymer network is done by thermally induce phase separation at -20°C , this gelation step is responsible for the final aerogel structure.

The results Cardea *et al.* obtained show that there is a maximum concentration of chitosan for the formation of hydrogels at low temperatures for which the solution falls into the gelation region, this region size increases with the decreasing of temperatures [87]. In addition, it is demonstrated that chitosan hydrogels that undergo through a solvent exchange at -20°C preserve their gel structure as opposed to solvent exchange at room temperature [86]. At this temperature gel remains in

a stable condition, which avoids any stress induced by acetone/water substitution at metastable conditions. Similar results are obtained by Li *et al.* [88] in the production of nanocellulose aerogels from a frozen aqueous solution at $-72\text{ }^{\circ}\text{C}$ followed by solvent exchange with 2-propanol at $-20\text{ }^{\circ}\text{C}$ and dried under ambient pressure at $70\text{ }^{\circ}\text{C}$. Results show that surface area is higher and shrinkage is lower when freezing is done instead of ambient temperature and the possibility to reproduce this results with other polysaccharides.

In addition, it has been reported the influence of the solvent in the final pore size, Jin *et al.* [89] and Ishida *et al.* [90] have reported higher specific surface area when *tert*-butanol (TBA) is used in a freeze-drying process. Lozinsky *et al.* [91] developed gelatin-based wide pore structures freezing a solution of Type A gelatin in DMSO followed by solvent exchange with cold EtOH at $-20\text{ }^{\circ}\text{C}$. Ching Ma [8] points out the relation between polymer concentration and SSA, and how the addition of urea that disrupt the hydrogen bonds creates a positive impact in the aerogel. In this work an agarose aerogel with a $\text{SSA} = 250 \pm 43\text{ m}^2\text{ g}^{-1}$ was developed by a similar route, frozen solution of agarose in DMSO frozen, cryoextraction with EtOH at $-28\text{ }^{\circ}\text{C}$ and scCO_2 drying at 120 bar and $50\text{ }^{\circ}\text{C}$.

These new approach for polymer aerogel preparation has the advantage that there is no sol-gel mechanism involved. Hence, materials that usually are not able to gel, can create gels whose porous structure is only caused by the frozen solution, with no additional cross-linkers or chemicals used for their production. However, polymers must be soluble in the solvent and their structure should not deteriorate with the anti-solvent.

Furthermore, Borisova *et al.* [92] reported that when using a aqueous solution of TBA, at the eutectic point, for the production of aerogels with freeze-drying, the

best mesoporous textural properties are achieved. Thus, the relation between the phase diagram water-TBA and the meso- and macropore ratios is confirmed and the possibility of controlling pore characteristics. This result is explained by the nature of crystals at eutectic points that are very small and also their solidification inside of the pores is less damaging than those solution non-eutectic. Yanagisawa *et al.* [93] indicates that solvent extraction from frozen aqueous phases allows a reduction of solvent and also extraction at low temperatures reduces the risk of solute decomposition and volatilization of organic solvents.

Dissolution and freezing with a posterior solvent exchange carried out under low temperatures is also reported in the production of porous membranes, a method called freeze-extraction. Morales-Román *et al.* [94] points out the relation of porosity with the concentration of polymer producing membrane of Poly(vinylidene fluoride) by freezing a solution of Poly(vinylidene fluoride) in N,N-dimethylformamide at $-80\text{ }^{\circ}\text{C}$ and a further solvent extraction with EtOH at the same temperature.

In addition, as pointed out by some authors, pore shape and size is determined by the template crystal of the solvent formed during the freezing step. In terms of their shape, during the freezing step if the sample is exposed to a gradient of temperature the ice forms elongated crystals because of constitutional supercooling at the ice-water interface [95]. Voges *et al.* [96] studies the preparation of a porous PVA material with freeze casting technique, based on temperature gradient. Some important results are: (1) the material presents an anisotropic pore structure Figure 2.14, due to the expected behaviour of water during freezing, (2) concentrations higher than 10 wt % are impossible to dry completely and concentrations lower than 5 wt % are not stable, (3) independence of concentration in pore size distribution. Zhang *et al.* [97] has developed a foam (APPF) with vertical oriented pores with via freeze-

extraction, in this case the solvent in which PAN is dissolved is DMSO and the temperature for the extraction is -20°C . Some relevant results are opposite to what is observed in [96], when increasing PAN concentration, pore size and distribution decrease being the pore size lowest at 9 wt %, Figure 2.15.

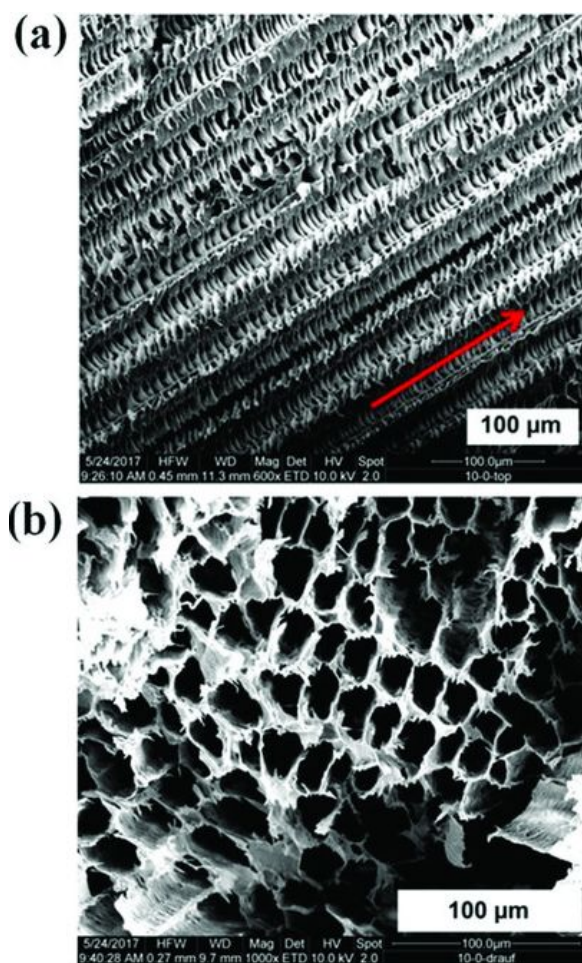


Figure 2.14: SEM images of the pore structure of the material. a) Lateral view of 10 wt% PVA. Freezing direction highlighted with a red arrow. b) Axial view. Reprinted from [96].

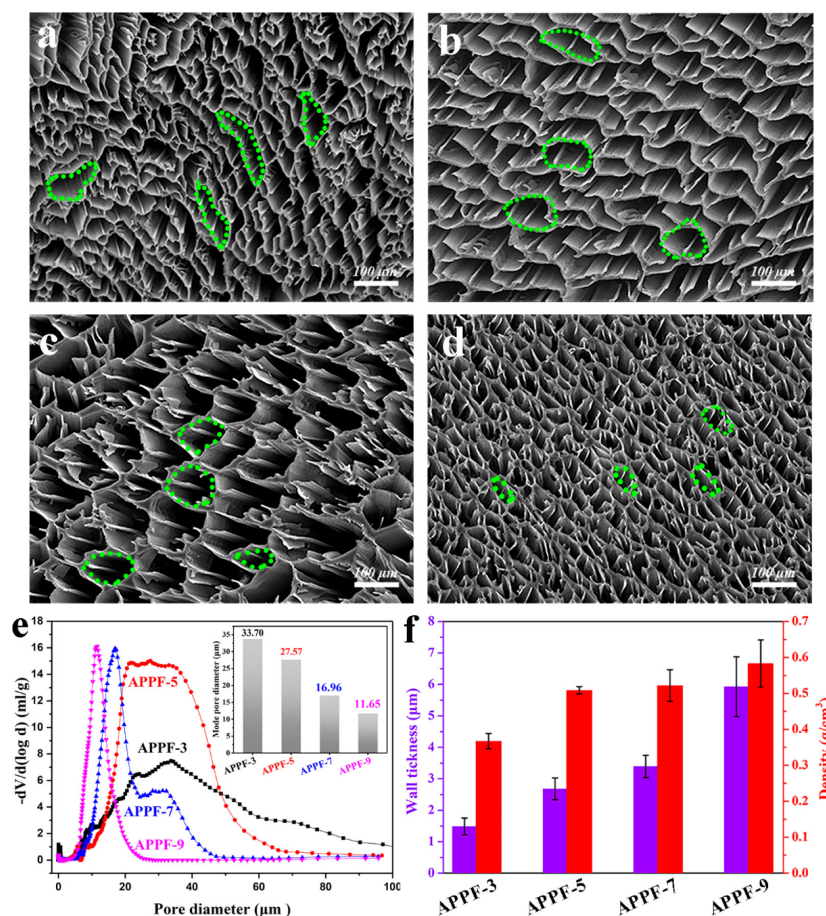


Figure 2.15: SEM images of (a) APPF-3, (b) APPF-5, (c) APPF-7, and (d) APPF-9 at the transverse cross-section (green dashed lines represent the pores in APPFs). (e) Pore size distribution of APPF-3, APPF-5, APPF-7, and APPF-9 as measured by Hg intrusion porosimetry. (f) Average thickness of the wall adjacent to the pores and the bulk density of APPFs vs PAN concentration. Reprinted from [97].

2.4.2 Screening of solvent and anti-solvent

Aerogels can be prepared from biopolymers (i.e. pectin, cellulose, chitosan, alginate, agar, gelatin, etc). Many studies have been done for their production by the preparation of a hydrogel in an aqueous solution followed by solvent exchange with EtOH and drying [98]. When taking into account solvent recycling in the process of solvent exchange for the hydrogel, if the solvent is EtOH an azeotrope is formed at 96 wt % what makes a simple distillation insufficient, therefore, another alternatives must be

used [99]. For this reason, another solvent has been explored that meet some requisites, miscibility with a wide range of organic solvents, non-toxic, melting point in a certain range (-25 – 25 °C), easy separation from EtOH which is commonly used in solvent exchange and the ability of dissolving biopolymers and other polymers.

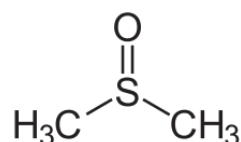


Figure 2.16: Molecular structure of DMSO.

Considering the requisites previously mentioned, dimethyl sulfoxide (DMSO) could be a feasible option. DMSO is an amphipathic molecule with a highly polar domain and two apolar groups being soluble in both aqueous and organic media, Figure 2.16. It is an efficient solvent for water insoluble compounds and it is a hydrogen-bond disrupter [100]. Its fusion temperature is 18.5 °C and boiling point 189 °C at 1 atm [101]. Due to the low toxicity, depending on the concentration, it has been used in biological studies and as a drug carrier [100]. In addition to those properties, DMSO can dissolve a great number of polymers.

Table 2.1: Solvents in which polymers are soluble

Polymer	Solvent
PAN	N,N'-dimethylformamide (DMF), DMSO, N,N'-dimethylacetamide(DMAc) [102], ethylene carbonate [103]
PVA	Water, water-miscible solvents(DMSO, glycerin, ethylen glycol) [104]
Inulin	DMSO [105]
Pectin	Water
Gum arabic	Water
CMC	Water

The anti-solvent must meet some requisites in order to get the best properties of the aerogels at the end of the process. These requisites have been already discussed in section 2.2.4.2. EtOH is the solvent selected due to its low price, non-toxicity, their successful use by some authors as an anti-solvent in a DMSO/EtOH system in the preparation of biopolymer aerogels [106], and its low melting point ($T_m = -117.3^\circ\text{C}$) that allows cryoextraction at -28°C .

2.4.3 Characterization of aerogels

2.4.3.1 Measurement of specific surface area (SSA)

The Brunauer-Emmett-Teller (BET) theory aims to provide an explanation for the physical adsorption of gas on a solid surface at low temperatures and it is used for the measurement of specific surface area of a material [107]. This theory was first published in 1938 by Stephen Brunauer, Paul Hugh Emmett, and Edward Teller. This theory is an extended multilayer theory of Langmuir's kinetic monolayer physical adsorption theory (1916). The BET theory refers to a multilayer adsorption using noncorrosive gases, such as nitrogen, argon, carbon dioxide as adsorbates [108]. This model considers that the adsorbed molecules in the first layer act as adsorption sites for the next layer, and at any pressure below the saturation vapour pressure p_0 , fractions of the surface are covered by layers of adsorbed molecules [109]. The specific surface area defined in this theory comprises both internal and outward surface area, but for pores that are closed specific surface area can not be determined. The description of the BET isotherm in a linear form is shown in Equation 2.1.

$$\frac{p/p_0}{V(1-p/p_0)} = \frac{1}{V_m C} + \frac{p/p_0(C-1)}{V_m c} \quad (2.1)$$

V is the volume of the adsorbate, V_m is the volume of the amount of adsorbate required to shape a monolayer, and C is the equilibrium constant used in the Langmuir isotherm improved by the vapour pressure of the adsorbate. Parameter C is exponentially related to the first-layer adsorption energy. The plot of Equation 2.1 in the form of $p/[V(p_0 - p)]$ versus p/p_0 should give a straight line with slope $s = (C - 1)/V_m C$ and intercept $i = 1/V_m C$.

The validity of this theory for measurement of specific surface area is limited to a certain range of relative pressure, Figure 2.17. Brunauer *et al.* found that the range in which the isotherm gave linear BET plots was $p/p_0 = 0.05 - 0.35$. Later research has shown that this range is too wide, and some deviations from linearity start at $p/p_0 \sim 0.25$ [110].

This validity pressure range is because of the initial assumptions made in the theory [111]:

1. Adsorption occurs only on well defined sites of the surface with one per molecule.
2. A molecule can act as a single adsorption site for a molecule of the upper layer.
3. The uppermost molecule layer is in equilibrium with the gas phase, i.e, the same adsorption and desorption rates.
4. The desorption is kinetically limited and is homogeneous, the same heat of adsorption for a given molecular layer, layers greater than the first layer have a heat of adsorption equal to the heat of liquefaction.
5. At saturation the layer number tend to infinity, equivalent to the sample being

surrounded by a liquid layer.

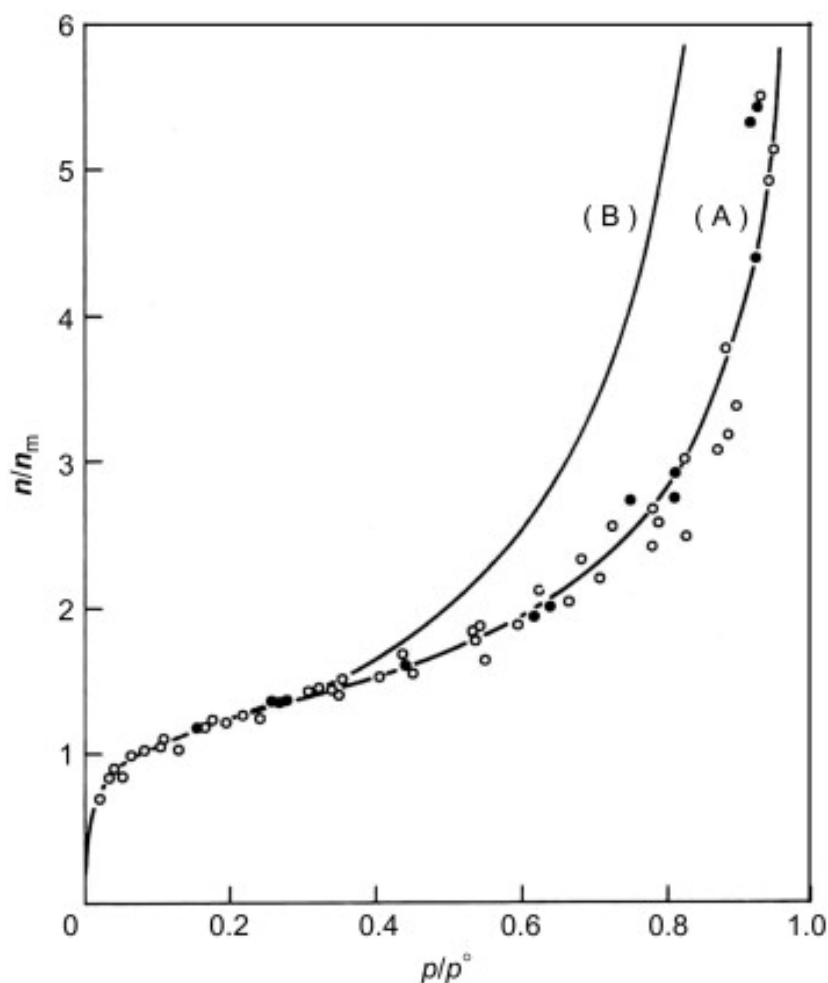


Figure 2.17: Curve (A) adsorption isotherms of nitrogen at 77 K on non-porous silicas and aluminas. Curve (B) adsorption isotherm calculated from equation. Reprinted from [109].

2.4.3.2 Scanning electron microscopy (SEM)

Scanning electron microscopy is a technique widely used to analyze the morphology of a material. It is widely used due to the high resolution that can be obtained, of the order of 1–5 nm and the very high magnification range (10–500000 times). This technique produces images of a sample by scanning it with a beam of electrons. The interactions produced between the material and the electrons can be divided into

two different categories: elastic and inelastic interactions. Elastic scattering result from the deflection of the electron by the atomic nucleus or outer shell electrons of the sample, electrons that are elastically scattered are called backscattered electrons (BSE) and yield a useful signal for imaging the sample. Inelastic scattering occurs through a variety of interactions between the incident electrons and the electrons and atoms of the sample, during this interaction specimen atoms are ionized and generate secondary electrons (SE). Both signals are primarily used to form and image but they are not the only signals produced during the process, other signals are, characteristic X-rays, Auger electrons, and cathodoluminescence (CL) [112]. These signals are collected by various detectors in the chamber, these detectors can be for SE, BSE signal detection and/or X-ray spectrometers. Modern SEMs devices have detector for these three signals [113].

Features analyzed by SEM are specimen shape, within this category some of its applications are examining porosity (size, distribution), measuring particles and microstructural feature sizes and distribution; quantification of chemical composition measured by BSE imaging or X-ray spectroscopy; surface crystallography carried out by electron backscatter diffraction [113].

3. Materials and methods

3.1 Materials

Chemicals used in this study have been listed in Table 3.1

Table 3.1: List of chemicals used in this study.

Chemical	Supplier	Purity
Alginic acid ammonium salt	Carl ROTH	
Xanthan (E-415)	Carl ROTH	
Gummi arabicum	Carl ROTH	
CMC sodium salt (low viscosity)	SIGMA Aldrich	
CMC sodium salt (medium viscosity)	SIGMA Aldrich	
Phytigel	SIGMA Aldrich	
Guar Flour	Carl ROTH	
Agar - Agar	Carl ROTH	
<i>ι</i> -Carrageenan	Gelcarin GP 379 NF	
<i>κ</i> -Carrageenan	Gelcarin GP 911 NF	
<i>λ</i> -Carrageenan	Viscari GP 109 NF	
Polyacrylonitrile (PAN)		
Pektin Amid	Herbstreith & Fox KG	
Polyvinyl alcohol (PVA)	SIGMA Aldrich	MKCK8710
Inulin	Orafti GR	
Dimethyl sulfoxide	Merk	≥ 99%
Ethanol	Carl Roth	≥ 99.5%
<i>tert</i> -Butanol	Carl Roth	≥ 99%

3.2 Preparation of aerogels

In this section it is explained the innovative route followed for the preparation of aerogels. It was established a standardized route with PAN dissolved in DMSO. Some conditions were modified to study their effect on the final aerogel and reach optimal properties. These conditions were, moulds used for the preparation of the frozen sample, total weight of the sample and concentration of PAN (0.625–10 wt %).

The procedure followed for the preparation of the monoliths consisted in three different steps. First, dissolution of the polymers in the solvent, second, solvent exchange at $-28\text{ }^{\circ}\text{C}$ and third, scCO_2 drying. The scheme of the preparation route is shown in Figure 3.1

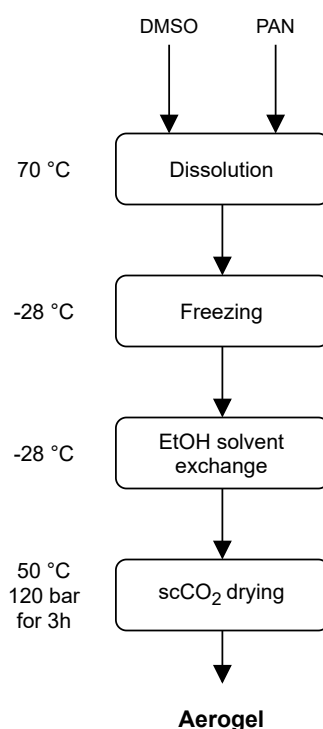


Figure 3.1: Preparation route for PAN aerogels.

3.2.1 Dissolution of polymers

Solvent was placed in a beaker covered with a watch glass to avoid evaporation, heated at 70 °C with constant stirring. When temperature was reached polymer was added in the exact quantity and kept the stirring at 70 °C until the polymer was completely dissolved. At that point, the solution was placed at room temperature until it cooled down and afterwards it was poured in an aluminium mould and placed inside of the freezer overnight at –28 °C.

3.2.2 Cryoextraction with ethanol

To carry out the extraction of DMSO, samples were carefully removed from the mould and placed in plastic containers filled with 100 ml ethanol at –28 °C and placed back in the freezer for 2 to 3 days. EtOH was replaced twice a day with a time difference of 5–6 h.

The objective of solvent exchange was to obtain an alcogel of EtOH and no DMSO. To check the concentration of DMSO in the samples a linear correlation between the density and the concentration was made. A calibration curve for DMSO/EtOH [8] and solution of TBA in water (20 wt %)/EtOH were used. Densities were measured by the density meter (DMA 4500 M, Anton Paar, Germany). Calibration curves were plotted, density versus concentration, Appendix 7.1.

After 3 days, 15 ml of the solution in the containers was taken out and placed at room temperature. Afterwards, concentration of EtOH was monitored with the density meter and calibration curves. If the concentration was ≤ 99 wt % cryoextraction was extended.

3.2.3 Supercritical CO₂ drying

To obtain final aerogels from alcogels supercritical drying was used. Once the alcogels were free of DMSO, they were measured, weighted and placed inside of teabags. Teabags were placed into the preheated 250 ml autoclave, Figure 3.2. After that, the autoclave was sealed and pressurized to 120 bar and 50 °C for 3 hours. During the process, scCO₂ mass flow rate was approximately 35 g/min. After 3 hours autoclave was depressurized and samples were taken out, weighted and measured. Each sample was placed in a sealed container and stored at room temperature.

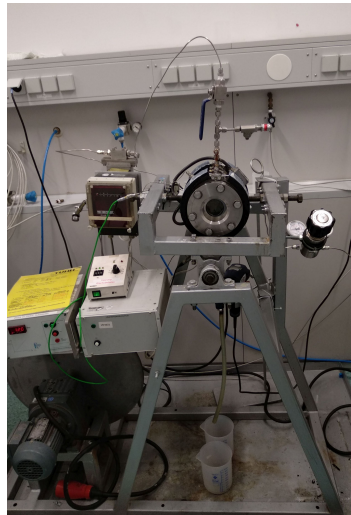


Figure 3.2: 250 ml autoclave for scCO₂ drying.

Volume shrinkage and linear shrinkage were calculated with Equation 3.1 and 3.2.

$$V_{shrinkage} = \frac{V_0 - V_1}{V_0} \cdot 100\% \quad (3.1)$$

where V_0 is volume after DMSO extraction and V_1 is volume after scCO₂ drying.

$$L_{shrinkage} = \frac{D_0 - D_1}{D_0} \cdot 100\% \quad (3.2)$$

where D_0 is volume before and D_1 is volume after the process. It was calculated for both cryoextraction and scCO₂ drying.

Porosity is calculated with Equation 3.3

$$\varepsilon = 1 - \frac{\rho_{bulk}}{\rho_{skeletal}} \quad (3.3)$$

where ρ_{bulk} is the density of the monolith calculated with its volume and grams, and $\rho_{skeletal}$ is different for each polymer and are listed in Table 7.1. When there are more than one polymer, the weighted average is used in $\rho_{skeletal}$.

In addition, urea was added at different concentrations to modify the properties of the aerogel. First of all, the solution of PAN at different concentration (5 and 7.5 wt %) was prepared following the method already described. Solution was let to cool down to 50 °C and urea was added at different concentrations 1, 2 and 4 wt %, this concentration relates to the already prepared 5 and 7.5 wt % solution, under constant stirring. Once urea was dissolved, it was transferred to the freezing mould to froze. Afterwards the standard route was followed.

Furthermore, PVA and agar-agar where combined with PAN at different concentrations. Total polymer concentration was 5 and 7.5 wt % and the polymer ratio was 50% for agar-agar and 25, 50, 75% for PVA. It was prepared by dissolving the exact amount of PAN in DMSO at 70 °C followed by the addition of the other polymer and its dissolution under constant stirring at 70 °C. After this point the standard route was followed.

3.3 Screening of process variables

In this section it is explained all the variables studied and the method used in order to achieve an aerogel with better properties.

3.3.1 Solubility of polymers in DMSO and TBA

Solubility was analysed visually at room temperature with the following procedure. Into a closed container 19 g of DMSO were poured. Solubility at 70 °C were test for 5 wt % if polymer was not soluble at this concentration, concentration was lowered to 1 wt % and the procedure was repeated.

Polymers that were not soluble in DMSO with a concentration of 1 wt % were tested again but changing the solvent to a 20 wt % aqueous solution of *tert*-butanol (TBA). Same procedure was followed but the concentrations were 3 wt % and 1.5 wt %. Polymers that could be dissolved were further prepared as described in section 3.2.

3.3.2 Freezing moulds

Different freezing moulds were analyzed. All the moulds tested are shown in Figure 3.3. In addition to these moulds, cell culture plate size 6 wells were also used. The route followed after freezing is the one described in section 3.2.

p Candle moulds were preconditioned flattening the surface before pouring any solution. Polymers PAN, PVA and pectin amid were tested in syringe moulds. Every polymer listed in Table 3.1 was tested in aluminium plates. Candle and hard moulds were only tested for PVA and PAN.

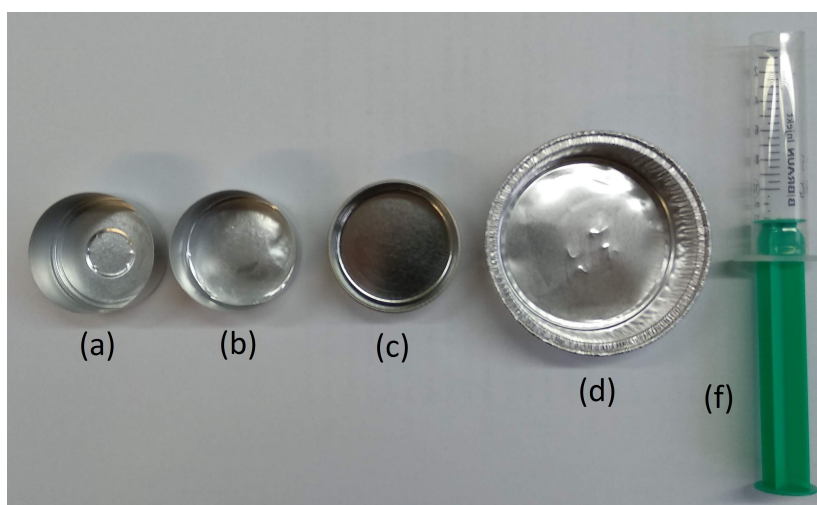


Figure 3.3: Moulds tested for the preparation of aerogels: (a) Candle mould before preconditioning (b) Candle mould (c) Hard mould (d) Aluminium plate (f) Plastic syringe.



Figure 3.4: Cell culture plate size 6 wells.

3.3.3 Thickness of monolith

Variation of the thickness was studied through the quantity of sample that was poured into the mould, samples of 5 g and 10 g were compared for concentrations of PAN in the range of (2.5 – 10 wt %).

3.3.4 Freezing temperature

To study the effect of freezing rate solutions were frozen at two different temperatures. The first temperature analyzed was $-28\text{ }^{\circ}\text{C}$, mentioned in the standard route for the preparation. Second temperature analyzed was $-196\text{ }^{\circ}\text{C}$. For the later, samples were placed in the mould and afterwards they were immersed in liquid nitrogen for 1–2 min making sure that the sample was visually frozen. Samples already frozen were finally placed overnight inside of the freezer at $-28\text{ }^{\circ}\text{C}$. The next steps were the same mentioned in section 3.2. In addition to monoliths, particles were produced by carefully placing droplets of polymer solution with a plastic syringe in the surface of moulds that were immersed in liquid nitrogen.

3.4 Characterization of aerogels

The quality of the samples produced, changing concentration, moulds and size, was mainly quantified by the analysis of the specific surface area with Braunauer-Emmett-Teller (BET) adsorption isotherm.

3.4.1 BET adsorption isotherm

Specific surface area (SSA) was measured by N_2 adsorption following the Brunauer-Emmett-Teller (BET) theory, section 2.4.3. For this measurement a surface area and pore size analyzer was used (NOVA 4000e, Quantachrom GmbH & Co. KG, Germany), Figure 3.5.

First of all, 20–30 mg from the center of the aerogel were placed inside of an empty cell that was previously weighted. Afterwards and before carrying out the measure-



Figure 3.5: Surface area and pore size analyzer NOVA 4000e.

ments, it underwent into a degassing process for 10 h to remove moisture and any trace of solvent that could remain in the sample. After that period, cells were cooled down to room temperature and weighted to calculate sample's weight by difference with the empty cell weight.

To measure SSA, four cells were loaded in the device and liquid nitrogen was poured into the device's container. The measurement for SSA was done only for 6 points and lasted around two hours. The device recorded and analyzed the data on Novawin software. Final results of SSA were retrieved and if the correlation coefficient of Equation 2.1 was $R^2 \geq 0.999$ results were taken as valid, if not data point selection was made in order to get $R^2 \geq 0.999$.

3.4.2 Scanning electron microscopy

The morphology of the aerogels that had high SSA was characterized by SEM. The field emission gun scanning electron microscopy (FEG-SEM) was conducted on an electron microscope (SUPRATM 55 VP, Zeiss, Germany). Samples were fixed on a sample holder and coated with a gold/palladium (Au/Pd) layer (approximately 10 nm) using a sputter coater. Subsequently, the micrographs of the prepared samples were taken at an acceleration voltage of 15 kV.

4. Results and discussion

4.1 Different polymers

This section shows the behaviour and properties of aerogels from different polymers prepared with the standard route. The aim of this part is to establish a starting point in the selection of polymer for a study in depth of multiple variables.

4.1.1 Solubility

Among all the polymers tested, solubility in DMSO at different concentrations (5 wt % and 1 wt %) was successful for Phytigel, PAN, PVA, inulin, gum arabic, guar flour, agar-agar, k-carrageenan. Polymers insoluble in DMSO were soluble in aqueous TBA (20 wt %) at different concentrations. All the polymers tested and the solvent in which they are soluble are listed in Table 4.1.

Although every polymer is soluble at least in one solvent, solution viscosity changes with concentration. Xanthan and *l*-carrageenan at 1 wt % have very high viscosity and are not studied further.

Table 4.1: Polymers soluble in DMSO and TBA/Water.

DMSO	TBA/Water (20 wt%)
Gummi arabicum	Alginic acid ammonium salt
Phytigel	Xanthan (E-415)
Guar Flour	CMC sodium salt (low viscosity)
Agar-agar	CMC sodium salt (medium viscosity)
κ -Carrageenan	ι -Carrageenan
Polyacrylonitrile (PAN)	λ -Carrageenan
Poly(vinyl alcohol) (PVA)	Pektin Amid
Inulin	

4.1.2 Cryoextraction

During cryoextraction some polymers present a non-desired behaviour in ethanol. Inulin dissolves completely and agar-agar show some structural damage. DMSO is completely exchanged with ethanol after five changes, this process lasts approximately two and a half days.

Once DMSO is completely exchanged each sample has different appearance, variation in color, size and opacity. Not only visual differences but some are extremely fragile and difficult to handle. Hence, some monoliths are broken which makes it difficult, even impossible in some cases, to measure their dimensions. These polymers are: guar flour, gum arabic and CMC sodium salt low viscosity.

4.1.3 Properties of the gels

The results of linear shrinkage, density and specific surface area for different polymers aerogels prepared by the standard route are shown in Table 4.2.

In Table 4.2 the reason for conducting the experiments only once is because it was only an initial approach to check their properties and which polymers could form aerogels with no deterioration during the process. Concentration for the polymers was a first approach and in some cases it was lower due to high viscosity. According to the data shown in Table 4.2 a representation of SSA is made in Figure 4.1. The calculation of porosity is done with Equation 3.3 and skeletal densities for different polymers are in Table 7.1.

Table 4.2: Results of properties of different polymers' aerogels.

Polymer	Concentration (wt %)	$I_{\text{shrinkage}}$ (%)	Porosity (%)	SSA (m^2g^{-1})
PAN	5	9.5	94.1	161
Alginic acid	3	3.8	96.4	87
k-carrageenan	1	43.0	95.4	79
CMC Na salt low*	3	/	/	56
CMC Na salt med	3	28.1	95.8	55
Pectin amid	3	2.7	97.9	51
λ -carrageenan	3	16.7		38
PVA	5	26.0	85.6	33
Guar flour**	5	15.3		/
Phytigel**	1	48.0		/
Gum arabic*	5	/	/	/

*These polymers were broken after scCO_2 drying and were impossible to measure. ** SSA is very low and BET measurement retrieves erroneous result.

These results show that each polymer due to its properties and the relation with the solvent, have different specific surface area. Most of the polymers have a specific surface area below $80 \text{ m}^2 \text{ g}^{-1}$, which is lower compared to the common value of aerogels ($300\text{--}1500 \text{ m}^2 \text{ g}^{-1}$), section 2.2.4. One possible reason that could explain this is the presence of macropores over mesopores which are outside of the range of BET

analysis (2–50 nm, this explanation is based on the high porosity of all the aerogels (> 85%). One of the reasons could be owing to the natural property of different materials. Some biopolymers have higher intermolecular affinity (i.e. affinity between the molecules). They tend to form thicker walls during the freezing stage, leaving relatively large vacancies for DMSO crystals to grow. At the end, they form porous structures with high porosity but low SSA.

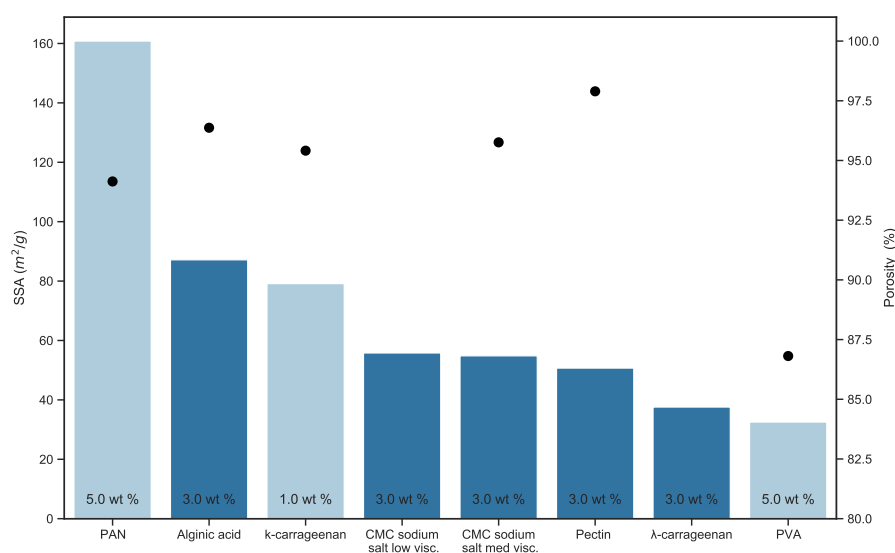


Figure 4.1: Comparison of specific surface area. ■ solvent DMSO ■ solvent TBA and ● porosity. Individual concentration is expressed in the correspondent bar.

Among all of the polymers tested, due to high specific surface area, relatively low shrinkage and performance, PAN is selected to be further studied.

4.2 PAN aerogels

After the initial study of different polymers, polyacrylonitrile (PAN) aerogels are studied at different concentrations (0.625, 1.25, 2.5, 5, 7.5 and 10 wt %). The aim of this part is to optimize certain parameters of the process to achieve aerogels with

the best quality. It is studied the effect that freezing mould, thickness of the monolith and freezing temperature have in the quality of PAN aerogels. Results of PAN aerogels at every concentration are shown in Table 4.3.

PAN aerogels at concentrations 1.25 wt % and lower experience a relative high shrinkage, a complete loss of their initial shape and SSA impossible to measure or extremely low. This behaviour is noticeable during solvent exchange where the gel becomes more delicate and difficult to handle in each change of solvent. Additionally, concentrations higher than 7.5 wt % present high viscosity which causes the removal of air bubbles inside of the solution before freezing almost impossible. Consequently, PAN aerogels outside of the concentration range 2.5–7.5 wt % were not studied in further experiments.

Table 4.3: PAN aerogel properties at different concentrations.

Concentration (wt %)	$V_{\text{shrinkage}}$ (%)	Porosity (%)	SSA (m^2g^{-1})
0.625	/	/	/
1.25	44.3	98.0 ± 0.3	40 ± 56
2.5	41.8 ± 8.1	96.9 ± 0.4	96 ± 36
5	36.8 ± 6.1	93.5 ± 0.6	119 ± 18
7.5	41.8 ± 1.3	90.8 ± 0.5	91 ± 14
10	34.2 ± 0.3	87.8 ± 0.4	42 ± 5

Volumetric shrinkage, porosity and specific surface area are shown in average \pm standard deviation. All of the experiments have been repeated at least three times.

In Figure 4.2 there is a comparison of PAN aerogels properties at different concentrations. Porosity decreases with the increase of concentration, this trend is also existent in volumetric shrinkage. However, there is an anomaly at 7.5 wt % where the volumetric shrinkage is higher than aerogels at 5 wt %. On one hand, low con-

concentrations allow more DMSO crystals to grow but pore walls are thinner which leads to higher volumetric shrinkage and on the other hand, higher polymer concentrations tend to form thicker pore walls, consequently, DMSO crystals are less numerous and bigger in size. The contribution of each phenomenon to specific surface area and pore size is still to be determined.

From Figure 4.3 linear shrinkage of PAN aerogels can be analysed. In concordance with what many authors have pointed out [7, 37, 35, 114] shrinkage of aerogels is caused by both solvent exchange and supercritical drying. However, in contrast to volumetric shrinkage, total linear shrinkage increases with the increase of the concentration. This could be explained by a higher shrinkage in the thickness at lower concentrations.

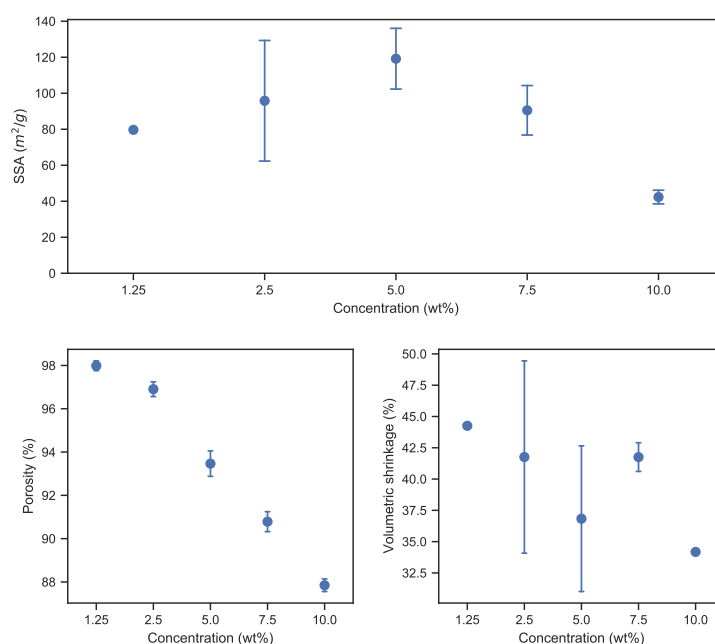


Figure 4.2: PAN aerogel properties at different concentrations.

The observed trend is opposite in each process, linear shrinkage experimented in

solvent exchange decreases with the concentration, whereas in scCO₂ drying increases. One of the possible reasons could be the direction in which solvent exchange is carried out, and the position of the monolith inside of the plastic containers. Furthermore, Takeshita *et al.* [115] proposes a mechanism that explains aerogel shrinkage during scCO₂ drying based on the low affinity between the polymer and CO₂ that produce coagulation between chains. These coagulated chains interact with each other by hydrogen bonds aggravating heterogeneous pore structure. They also point out that higher flows of CO₂ lead to higher shrinkage due to the formation mechanism.

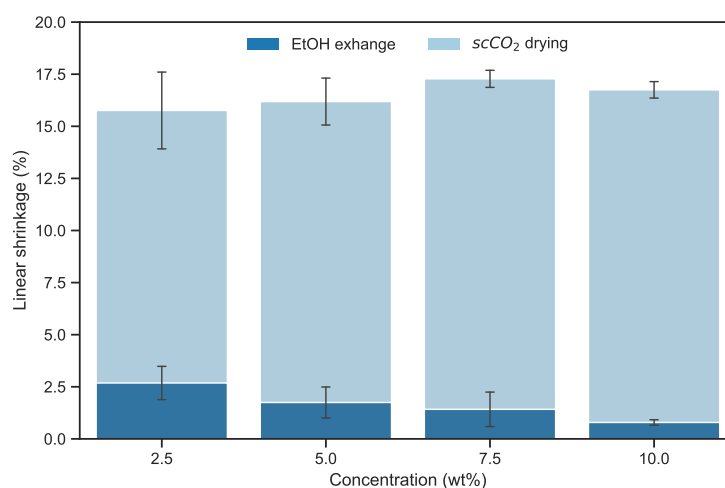


Figure 4.3: Comparison of linear shrinkage in solvent exchange and scCO₂ drying of PAN aerogels, ■ scCO₂ drying ■ EtOH exchange.

Moreover, aerogels have a convex surface, the outside of the monolith is thicker than the center, caused by the shrinkage during the process, Figure 4.5. Another feature visible in some samples is radial heterogeneity which is caused by two opposite phenomena. During freezing, small DMSO crystals grow and at the same time low thermal conductivity and heat capacity establish a limit of mass available of cooling that leads to radial heterogeneity. This effect has also been observed by Gutiérrez

et al. [116] in the preparation of PVA scaffolds at different freezing rates.

As a conclusion, PAN aerogels have a maximum specific surface area of $119 \pm 18 \text{ m}^2 \text{ g}^{-1}$ at 5 wt %. For concentrations lower than 2.5 wt % or higher than 10 wt % results are not good enough to explore them further. High standard error in volumetric shrinkage and SSA might be caused by human error introduced while measuring dimensions and the presence of macropores along with differences in pore structure due to directional freezing and small cooling rate that produces an anisotropic aerogel, Figure 4.6 and 4.7. In addition, another effect already mentioned by Aubert *et al.* [117] takes place, due to the design of the process polymer solution does not freeze instantly, consequently there is a bottom layer that is in contact with the cold surface that freezes first that creates an insulation effect with the solution on top leading to different pore structure between the bottom surface and the pore surface.

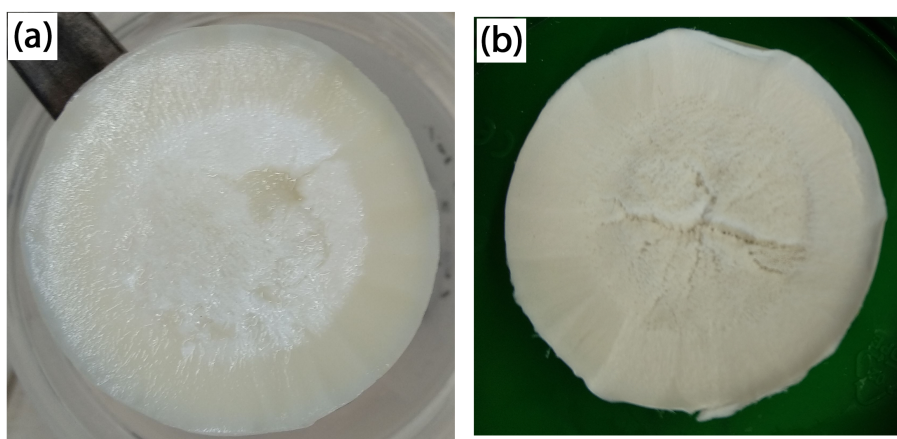


Figure 4.4: PAN aerogel 7.5 wt% with radial heterogeneity. (a) After solvent exchange (b) after supercritical drying.

As shown in Figure 4.6, 2.5 wt % aerogels present a hierarchical pore structure consisting in aligned rows, visible channels, interconnected through pores. Irregular shaped pores and their size distribution is wide, approximately they are in the range

of 200 nm. Furthermore, it is also perceptible a defined longitudinal shape of the pores. This phenomena supports the theory of directional freezing presented in section 2.4.1. Some possible reasons are low freezing rate, freezing from the bottom of the sample, unequal freezing due to differences of conductivity between the surface of the freezer, freezing mould and air.



Figure 4.5: PAN aerogel 5 wt%.

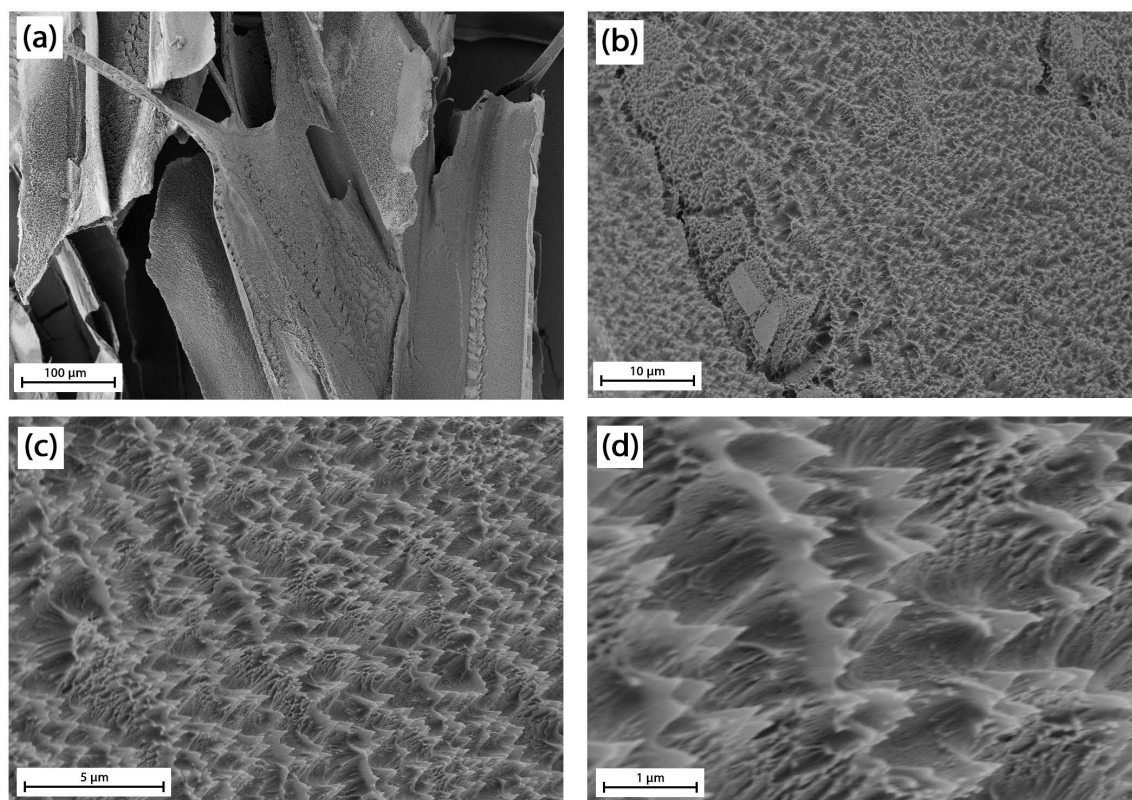


Figure 4.6: SEM images of PAN 2.5 wt% aerogel.

As shown in Figure 4.7 (b) and (e), 5 wt % aerogels present a heterogeneous morphology and wide range of pore size. Whereas in some parts pores are about 500 nm in size, in others 100 nm. Similarly to 2.5 wt% aerogels directional freezing is also present at this concentration. However there is not only one direction but multiple, Figure 4.7 (f) . This might be caused by crystallization heat and irregularities during freezing, possible hot spots and cold spots that create an uneven freezing surface. From Figure 4.7 (d), it can be seen that pore structure it is more uniform when it is closer to the skin of the aerogel.

According to SEM images pore structure is tighter and more regular than 2.5 wt % aerogels. Less PAN content allows DMSO crystals to grow freely in a looser structure where direction in pores is more accentuated.

4.2.1 Effects of the freezing mould

Selection of the mould between aluminium dishes, candle moulds, syringes, cell culture plate and hard moulds was done to see the effect it has on cryoextraction, final properties and also to make the shape and size of aerogel as reproducible as possible.

It is expected that the freezing rate of the gels in moulds of aluminium is higher than those of plastic due to its thermal conductivity. The highest the freezing rate the better for the creation of numerous smaller size pores [118].

In regards of freezing, whilst samples produced in disposable aluminium dishes and syringes are easily removed from the mould due to non constant diameter and non-stiff bottom material in the aluminium dishes and syringe's shape. Samples in the rest of the moulds require to begin solvent exchange with the gel in the mould,

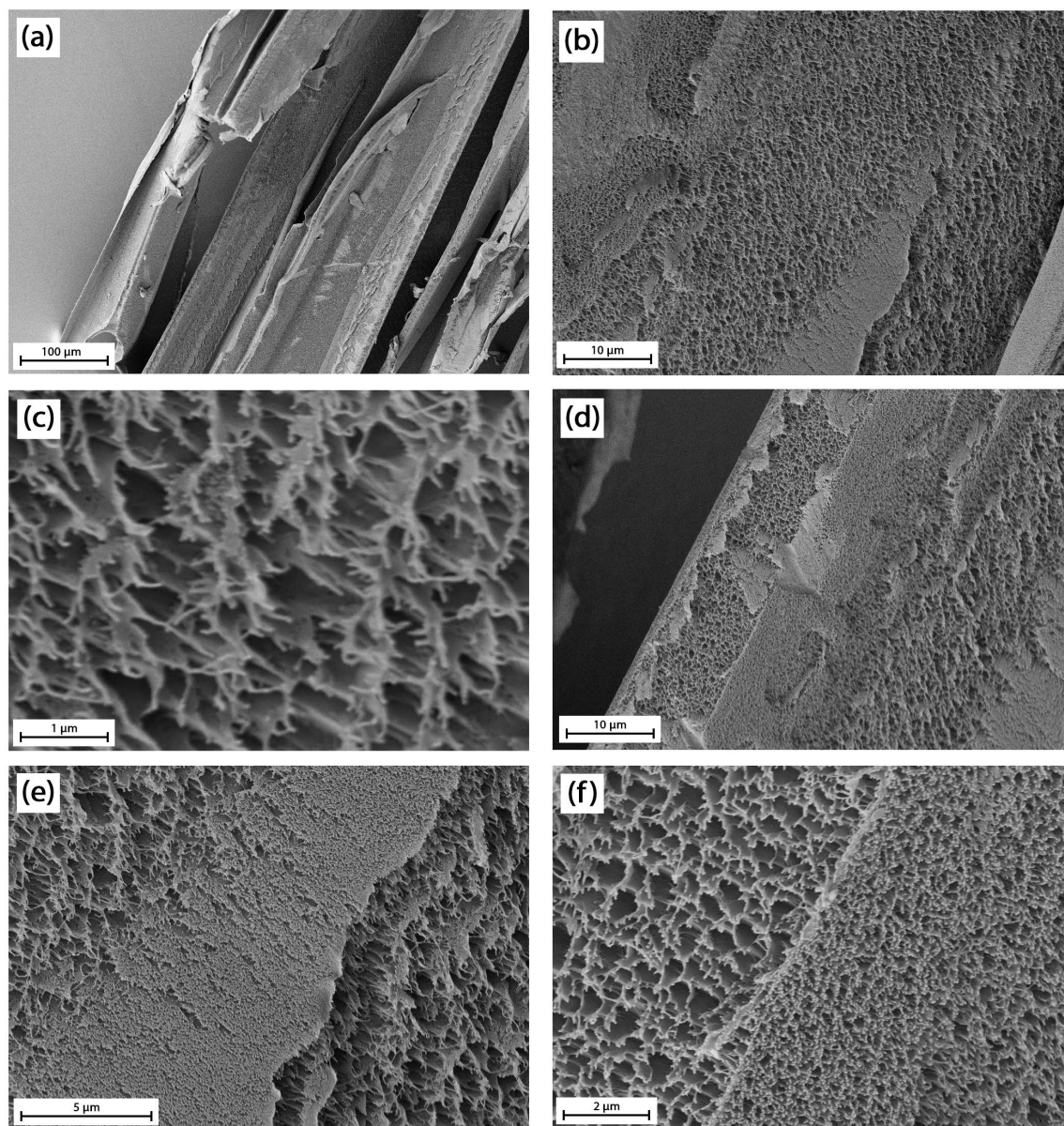


Figure 4.7: SEM images of PAN 5 wt% aerogel.

due to shrinkage observed during this step after one exchange gels can be removed. Moreover, samples in culture plates are very difficult to remove and have to be for a longer period in EtOH because of material's rigidity and even in some cases they can't be taken out due to minimum shrinkage. This aspect leads to nonuniform solvent exchange that might affect the final properties of the gel.

When samples are frozen in syringes, irregularities in its shape appear due to volume contraction while freezing and the direction of heat transfer. They present a hole in the center of the cylinder that during drying makes the samples at low concentrations collapse and lose its cylindrical shape, Figure 4.8 (a). These gels are fragile and difficult to handle during the process. Therefore, the use of syringes as freezing moulds is rejected.

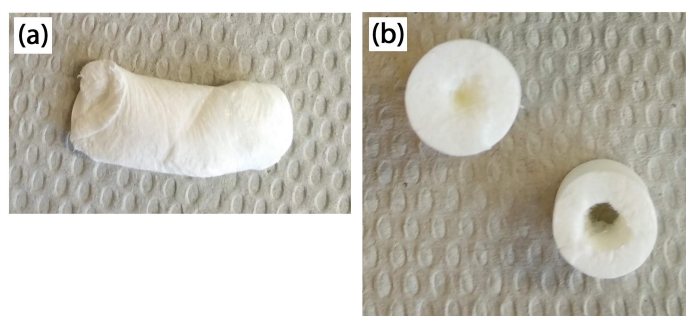


Figure 4.8: PAN aerogel in syringe: (a) 0.625 wt% (b) 5 wt%.

The results of the different moulds for PAN aerogels are shown in Table 4.4. Some moulds were tested only once because of bad results.

From Figure 4.9, freezing mould have an effect in specific surface area. When comparing candle and hard moulds, the later show a better result at every concentration, with a maximum of $120 \text{ m}^2 \text{ g}^{-1}$ at 5 wt %. One relevant result is that for each mould there is a maximum specific surface area at different concentrations of the polymer. This could be attributed to the different dimensions of the moulds. Thus, different

freezing rate for the same amount of sample.

In addition, taking into account not only measurable properties but also physical integrity during the process, ethanol consumption and reproducibility, the mould selected to achieve consistent results is the hard mould. Unlike candle moulds this one does not need any preconditioning, also the diameter of the mould remains constant and the surface is completely smooth after using it due to the material's stiffness. Overall it is the most convenient and it retrieves consistent results. However, in the case of polymers that show no shrinkage during solvent exchange, disposable aluminium dish are recommended to be used.

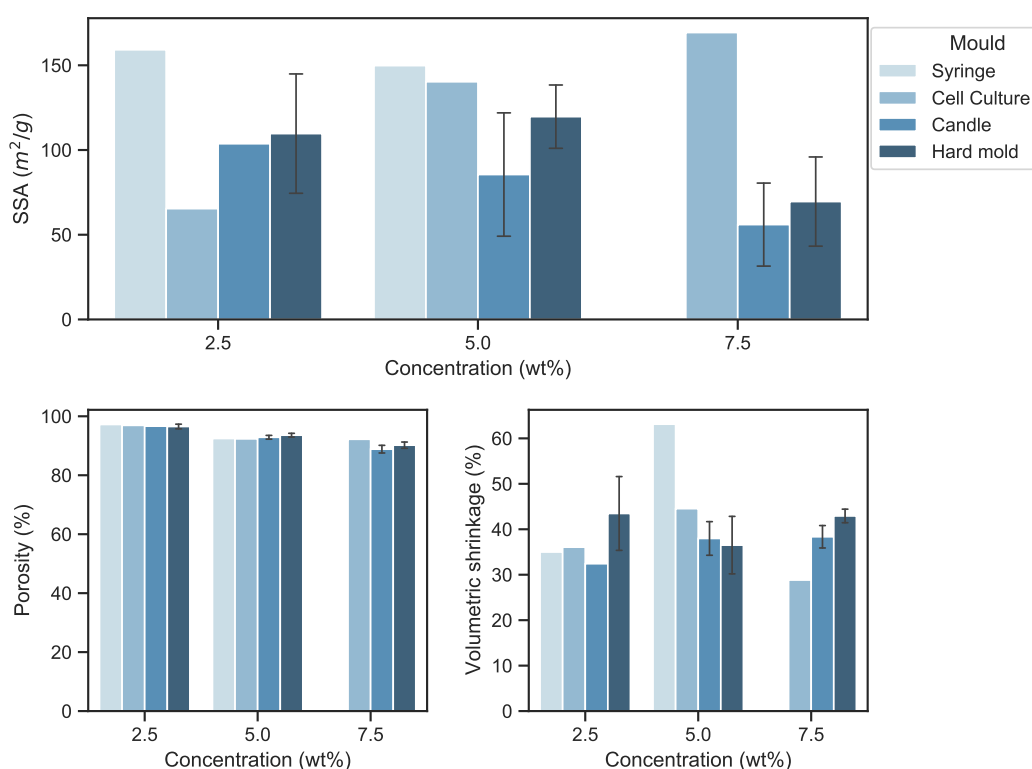


Figure 4.9: Comparison of specific surface area, density and volumetric shrinkage for different moulds.

Table 4.4: Results of PAN aerogels in different moulds.

Concentration (wt %)	Mould	V _{shrinkage} (%)	Porosity (%)	SSA (m ² g ⁻¹)
2.5	Candle*	32.4	96.7	104
	Cell Culture plate*	36.1	96.9	65
	Hard mould	43.5 ± 8.4	96.5 ± 0.8	110 ± 36
	Syringe*	35.0	97.2	159
5	Candle	38.0 ± 4.0	92.9 ± 0.7	86 ± 39
	Cell Culture plate*	44.5	92.3	140
	Hard mould	36.5 ± 6.9	93.6 ± 0.7	120 ± 21
	Syringe*	63.1	92.5	150
7.5	Candle	38.4 ± 2.7	88.8 ± 1.4	56 ± 27
	Cell Culture plate*	28.8	92.2	169
	Hard mould	42.9 ± 1.7	90.2 ± 1.2	67 ± 29
10	Candle	35.2 ± 1.7	86.4 ± 1.5	41 ± 4
	Cell Culture plate*	61.9	81.1	71

Volumetric shrinkage, porosity and specific surface area are shown in average±standard deviation. Experiments have been repeated at least three times.

* Only one value available due to bad results.

4.2.2 Thickness of the monolith

The effect thickness has on aerogel properties is mainly attributed to differences in the freezing rate. As it has been explained, increasing the freezing rate by lowering the thickness of the monolith, increases the number of pores and decreases pore size as explained in section 2.2.5.

Results obtained are in Table 4.5 and a graphical comparison of properties based on monolith thickness is in Figure 4.10.

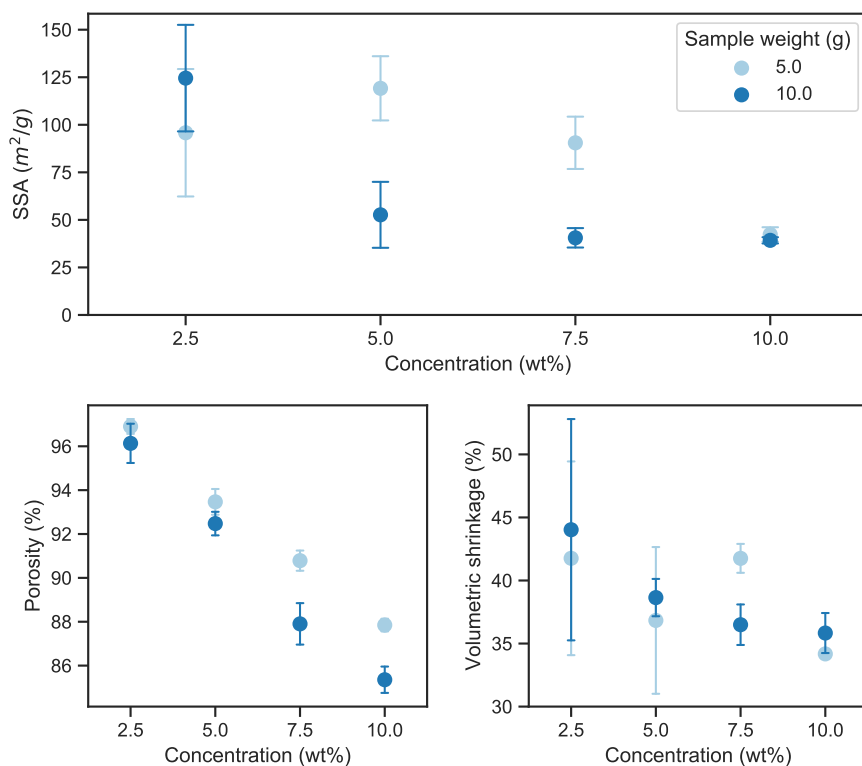


Figure 4.10: Comparison of specific surface area, porosity and volumetric shrinkage for different grams ■ 5g ■ 10g.

From Figure 4.10 the effect of the thickness in properties is clear. Although the biggest impact is in specific surface area, in porosity and shrinkage it has an effect too. Thicker samples are less porous and present a higher shrinkage. This could be explained by the increase in the thickness leads to more compact monoliths, thus, less space for DMSO crystals to grow with the consequent decrease in porosity.

In comparison to porosity and volumetric shrinkage, differences in specific surface area are noteworthy. Thinner samples at concentrations higher than 5 wt % have higher specific surface area. One of the possible reasons is that the lower thickness decreases the time for the sample to be frozen, therefore a higher freezing rate occurs. However, this reasoning can not explain the results at 2.5 wt %. While there

is a maximum at 5 wt % for samples of lower thickness, the maximum is located at 2.5 wt % for higher thickness samples. In addition, SSA remains constant approximately at concentrations higher than 7.5 wt %.

Table 4.5: Results of PAN aerogels with change is sample size.

Concentration (wt %)	Weight (g)	V _{shrinkage} (%)	Porosity (%)	SSA (m ² g ⁻¹)
2.5	5	41.7 ± 8.1	96.9 ± 0.3	96 ± 36
	10	44.0 ± 9.3	96.1 ± 0.9	125 ± 30
5	5	36.8 ± 6.1	93.4 ± 0.6	119 ± 18
	10	38.6 ± 1.7	92.4 ± 0.6	53 ± 20
7.5	5	41.7 ± 1.2	90.7 ± 0.5	91 ± 15
	10	36.4 ± 1.9	87.9 ± 1	41 ± 6
10	5	34.1 ± 0.2	87.8 ± 0.4	42 ± 5
	10	35.8 ± 1.9	85.3 ± 0.7	39 ± 2

Volumetric shrinkage, porosity and specific surface area are shown in average±standard deviation. All of the experiments have been repeated at least three times.

4.2.3 Effect of freezing temperature

The effect of freezing temperature was studied by submerging solutions of PAN aerogels of (2.5, 5 and 7.5 wt %) in liquid nitrogen at -196 °C until it was completely frozen.

All of the samples are frozen in less than 2 min, during this step freezing nucleus are visible at the bottom of the mould. These nucleus spread slowly and in some samples polymer chains at the surface are noticeable for a few seconds. During the period of placing samples at -28 °C after freezing in liquid nitrogen, some cracks

lengthwise appear in the surface, these are more pronounced through the solvent exchange. One reason could be that temperature gradient between ambient temperature and liquid nitrogen is too high and causes the polymer network to collapse. Low concentration samples show phase separation after their placement in the freezer overnight.

The duration of cryoextraction is equal to those prepared with the standard route, two and a half days. By the end of solvent exchange, gels are very fragile and some of them are broken which make impossible to measure their dimensions and only specific surface area can be quantified. Concentration has an effect in this non-desired behaviour, fragility increases with the decrease of concentration, even at early stages of solvent exchange samples are broken. One possible explanation for this is the formation of thinner and weaker pore walls with the decrease of concentration. Results of specific surface area, porosity and volumetric shrinkage are available in Table 4.6 .

Table 4.6: Results of PAN aerogels frozen with liquid nitrogen.

Concentration (wt %)	T_{FR} (°C)	V_{shrinkage} (%)	Porosity (%)	SSA (m²g⁻¹)
2.5	-28	41.8 ± 8.1	96.9 ± 0.4	96 ± 36
	-196	36.7*	97.2*	51 ± 17
5.0	-28	36.8 ± 6.1	93.5 ± 0.6	119 ± 18
	-196	35.2 ± 6.9	94.4 ± 0.0	56 ± 15
7.5	-28	41.8 ± 1.3	90.8 ± 0.5	91 ± 15
	-196	44.6 ± 6.3	90.8 ± 0.9	46 ± 10

Volumetric shrinkage, porosity and specific surface area are shown in average±standard deviation. Experiments have been repeated at least three times

* Only one value available due to structural damage.

From Figure 4.11, the use of liquid nitrogen as a freezing agent results in the decrease of specific surface area to less than $60 \text{ m}^2 \text{ g}^{-1}$ for every concentration. One possible explanation might be what has been reported by Wang *et al.* [119] in the preparation of nanostructured membranes of polyvinylidene fluoride (PVDF) by flash freezing. When a solution of a polymer in DMSO is immersed in liquid nitrogen, although initial crystals of DMSO are smaller, final pores are bigger than those with a lower freezing rate. The large freezing rate causes that polymer diffusion is essentially nonexistent. Therefore, initial DMSO crystal can agglomerate and grow resulting in big pores in the final material. The size of these pores is outside of the BET range (2–50 nm) what would explain the decrease in specific surface area.

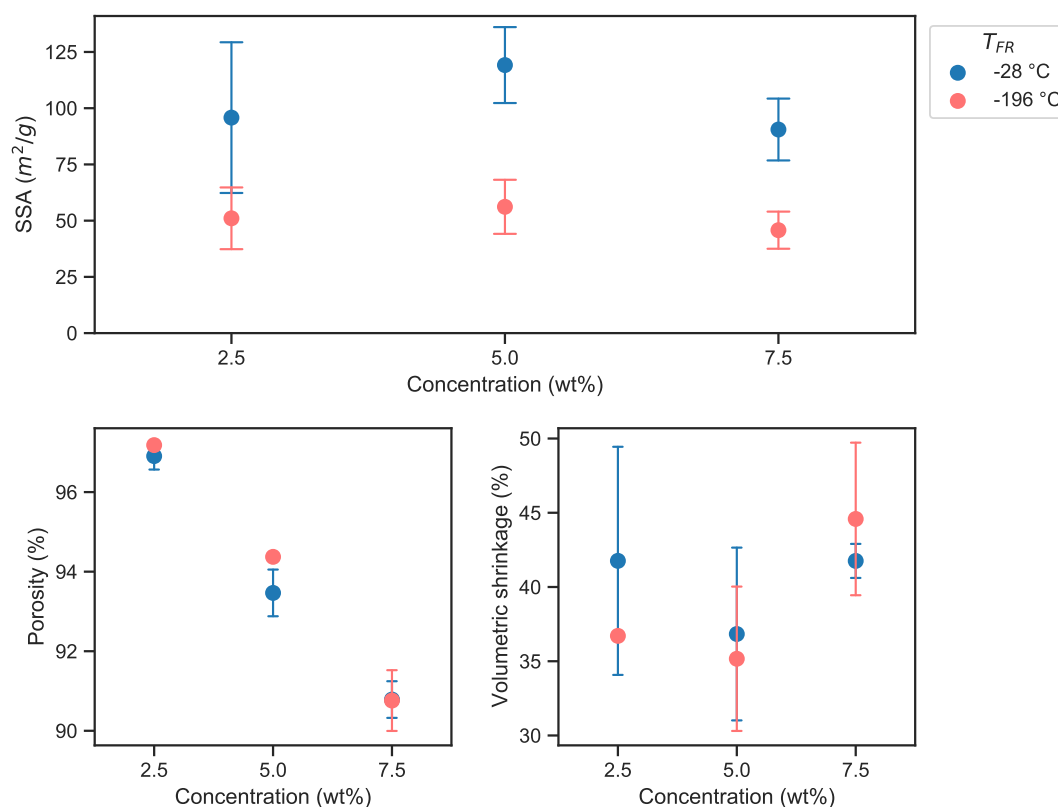


Figure 4.11: Comparison of specific surface area, porosity and volumetric shrinkage of PAN aerogels different freezing temperature ■ $-28 \text{ }^\circ\text{C}$ ■ $-196 \text{ }^\circ\text{C}$.

In addition, frozen sample undergo during a small period of time to ambient temperature before their placement inside the freezer at $-20\text{ }^{\circ}\text{C}$. This significant temperature gradient could create a fast and uncontrolled growing of initial smaller crystals that result in bigger size porous. Consequently, regions with different pore size might appear in the aerogel. This is another possible explanation for the decrease in specific surface area.

Changes in shape have an impact in specific surface area, particles in comparison to monoliths have a bigger surface area, $65\text{ m}^2\text{ g}^{-1}$ and $56 \pm 15\text{ m}^2\text{ g}^{-1}$ respectively. However, this value is still lower than 5 wt % aerogels frozen at $-28\text{ }^{\circ}\text{C}$ $119 \pm 18\text{ m}^2\text{ g}^{-1}$.

4.2.3.1 Morphology of the aerogels

As it is shown in Figure 4.12, aerogels prepared via flash freezing are heterogeneous materials, i.e. some parts present what seems to be dense, whereas other parts present a highly porous structure. This could be one of the reasons for the low specific surface area achieved. Additionally, porous structure is non-hierarchical what might suggest that glass transition might have been reached. Although results of the porous structure are promising there is no possibility to study whether the parts that look denser might have a porous structure below the surface or not.

In summary, aerogels frozen at $-196\text{ }^{\circ}\text{C}$ have an undesired physical behaviour where their physical integrity is compromised during the whole process. Although there are signs of non-hierarchical pore structure, specific surface area is $56 \pm 15\text{ m}^2\text{ g}^{-1}$ and porosity 94.4 %.

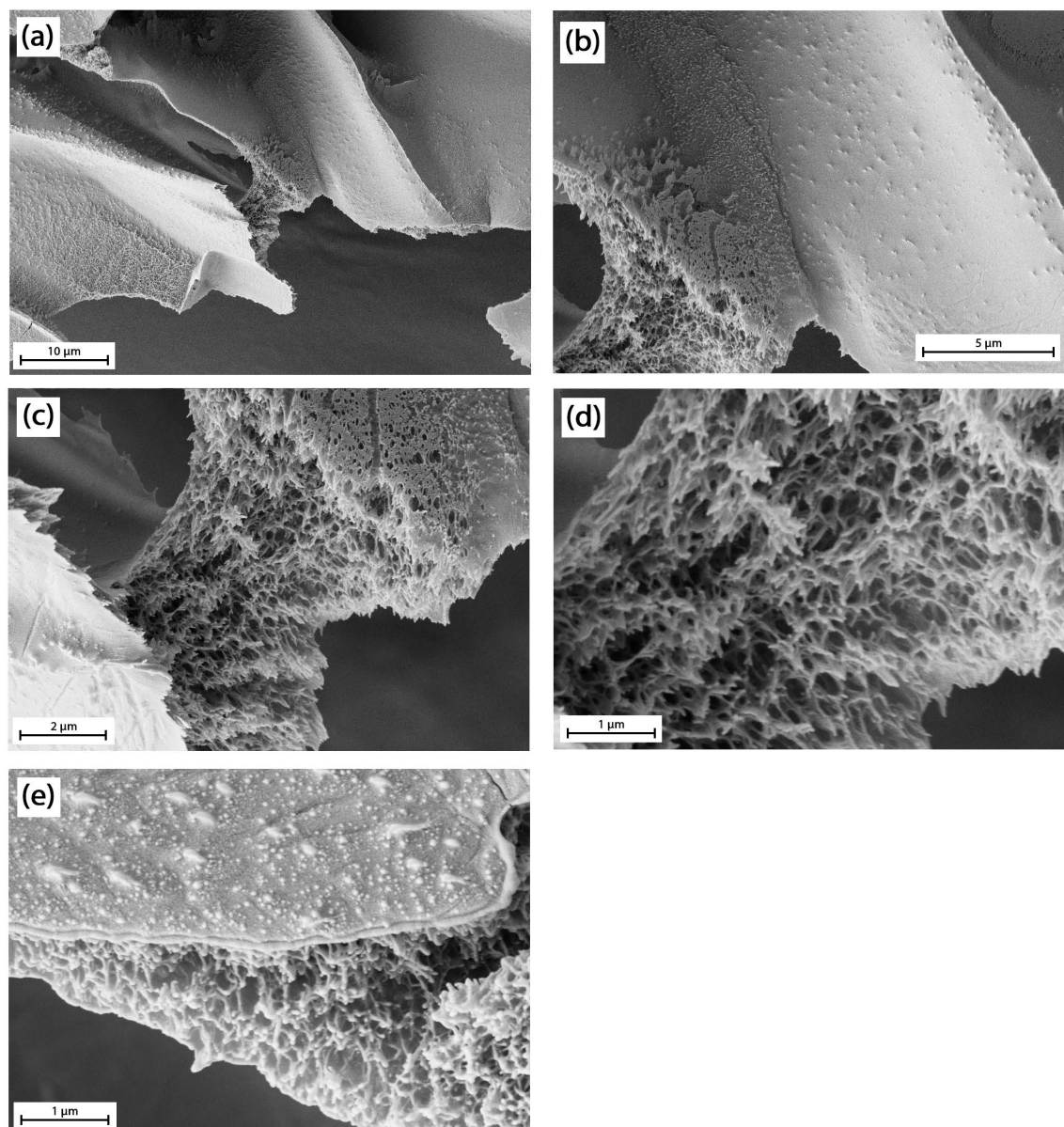


Figure 4.12: SEM images of PAN 5 wt% aerogel frozen at -196 °C.

4.3 PAN based aerogels

In this section addition of urea to PAN and multiples combinations of PVA and agar-agar with PAN for the preparation of aerogels are studied.

4.3.1 PAN/urea aerogels

The size of pore walls created by the polymer in the freezing stage have an effect on the size of DMSO crystals. This can be controlled by the reduction of hydrogen bonds between molecules with the addition of urea. Results for the addition of urea to PAN aerogels in 1, 2 and 4 wt %.

Table 4.7: Results of properties of hybrid PAN/urea aerogels at different compositions.

Material	Concentration (wt %)	$V_{\text{shrinkage}}$ (%)	Porosity (%)	SSA (m^2g^{-1})
PAN	5	36.8 ± 6.1	93.5 ± 0.6	119 ± 18
Urea/PAN	1/5	33.4 ± 3.8	95.2 ± 0.1	52 ± 8
	2/5	32.3 ± 2.8	94.5 ± 0.5	40 ± 23
	4/5	31.5 ± 4.6	95.2 ± 0.1	15 ± 15
PAN	7.5	41.8 ± 1.3	90.8 ± 0.5	91 ± 15
Urea/PAN	1/7.5	38.0 ± 2.4	90.6 ± 0.5	94 ± 18
	2/7.5	31.3 ± 7.4	90.9 ± 0.6	23 ± 32
	4/7.5	21.1 ± 5.5	92.6 ± 0.2	

Volumetric shrinkage, porosity and specific surface area are shown in average \pm standard deviation. All of the experiments have been repeated at least three times.

From Figure 4.13, specific surface area decreases with the increase of urea. The expected improvement due to the reduction of hydrogen bonds is non-existent. One possible reason could be that hydrogen bonds in PAN aerogels do not play a big role in the polymer network. Another reason could be that the crystallization of urea itself leads the creation of macropores, therefore, the increase in porosity with the addition of urea.

In terms of porosity and volumetric shrinkage, the addition of urea reduces volumetric shrinkage at both concentrations. Increasing the content of urea increases porosity and decreases volumetric shrinkage. However, the influence at 7.5 wt % is higher and volumetric shrinkage becomes constant at a value of $\sim 31\%$.

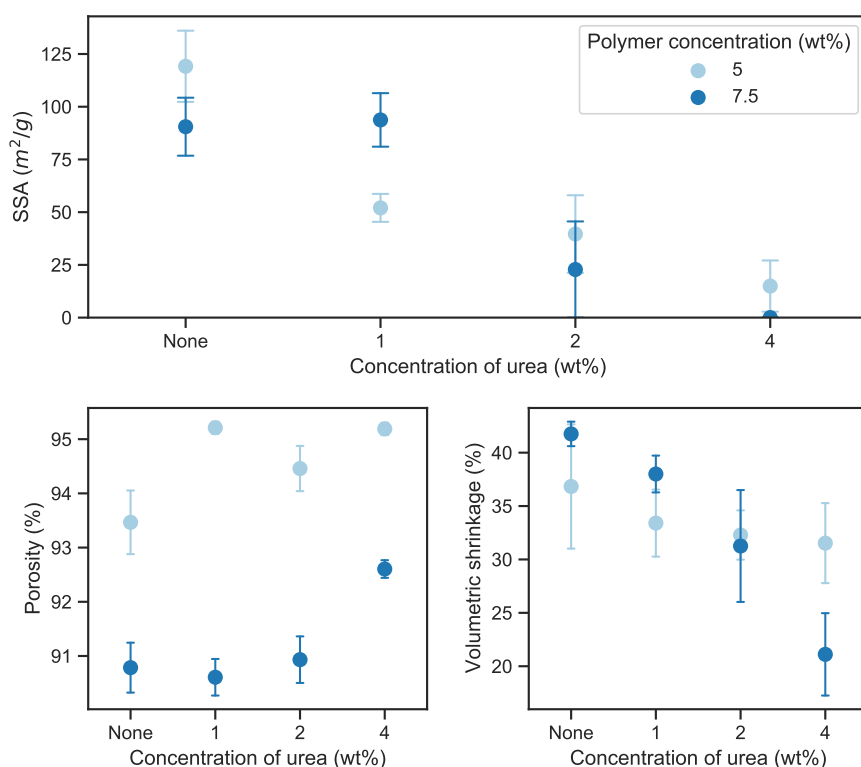


Figure 4.13: Comparison of specific surface area, porosity and volumetric shrinkage of PAN aerogels 5 wt% 7.5 wt% with the concentration of urea.

4.3.2 PAN/PVA aerogels

Blends of PAN and PVA have been studied in literature to combine both properties, mechanical and hydrophobicity from PAN and the potential biomedical and pharmaceutical applications of PVA due to the presence of OH groups and the possibility

of hydrogen bond formation with other chemicals. When they are mixed together, interactions with each other are expected to be through interchain hydrogen bonding [120].

Results of pure PAN and PVA aerogels are shown in Table 4.8, comparison of properties at different concentrations is in Figure 4.14.

Table 4.8: Results of properties of pure PAN and PVA aerogels at different compositions.

Concentration (wt %)	Material	$V_{\text{shrinkage}}$ (%)	Porosity (%)	SSA (m^2g^{-1})
2.5	PAN	41.8 ± 8.1	96.9 ± 0.4	96 ± 36
	PVA	53.6 ± 2.9	92.3 ± 1.6	43 ± 13
5.0	PAN	36.8 ± 6.1	93.5 ± 0.6	119 ± 18
	PVA	53.3 ± 5.1	90.1 ± 2.1	81 ± 38
7.5	PAN	41.8 ± 1.3	90.8 ± 0.5	91 ± 15
	PVA	47.7 ± 5.6	90.6 ± 3.9	107 ± 15
10.0	PAN	34.2 ± 0.3	87.8 ± 0.4	42 ± 5
	PVA	40.1 ± 5.2	85.8 ± 1.1	86 ± 32

Volumetric shrinkage, porosity and specific surface area are shown in average \pm standard deviation. All of the experiments have been repeated at least three times.

From Figure 4.14, specific surface area is maximum for different concentration depending on the polymer, for PAN is 5 wt % and for PVA 7.5 wt %. This difference is caused by the interaction between polymer and DMSO and the nature of polymer that leads to different pore structure and variation in pore walls. Moreover, volumetric shrinkage is higher and porosity lower for PVA aerogels at every concentration. One possible explanation is that pore walls in this case are thinner and hence collapse of the network is more severe, higher than 50% in some cases.

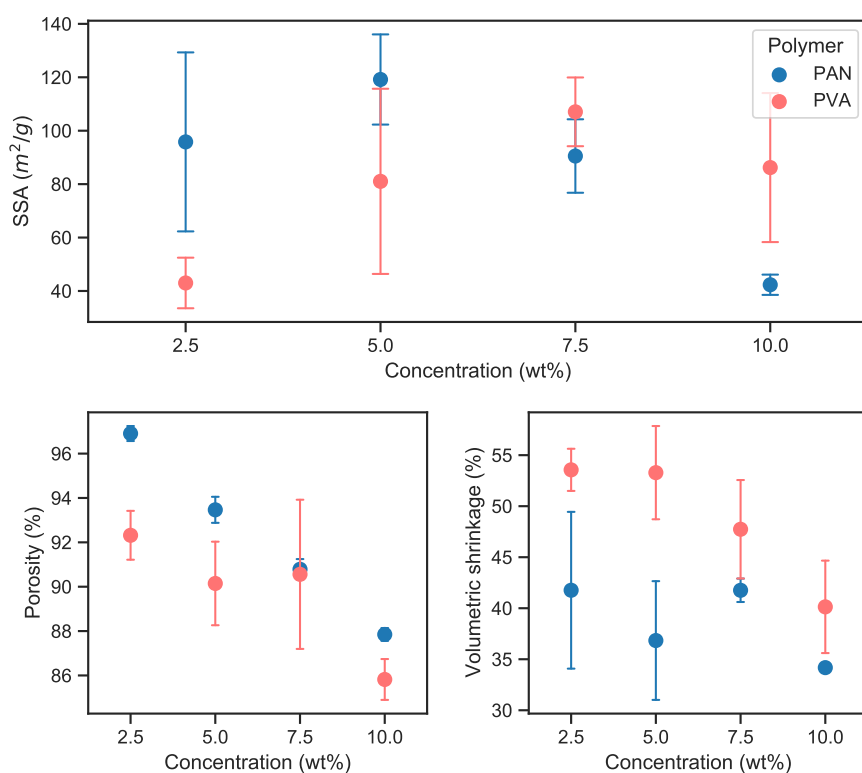


Figure 4.14: Comparison of specific surface area, density and volumetric shrinkage for ■ PAN and ■ PVA.

PAN was combined with PVA in solutions of 5 wt % and 7.5 wt % polymer content to see what are the effects of different PVA/PAN ratio in the properties of the aerogel. The results obtained are shown in Table 4.9.

In Figure 4.15 a comparison of different PVA/PAN aerogels can be seen. All of the aerogels have a concentration of 5 wt % and differ on the proportion of both polymers, being 0 and 100% entirely PAN and PVA respectively. Porosity decreases with the increase of PVA content in a non-linear form, the opposite trend is observed in linear shrinkage, increasing PVA content results in higher shrinkage.

Unlike porosity and linear shrinkage, specific surface area do not present any linear

trend versus PVA content, particularly for 25, 50 and 75% there is a slight increase. Overall, addition of PVA decreases specific surface area at every PVA concentration in comparison to aerogels made exclusively from PAN or PVA. These results may be related to the network created by the interaction of both polymers and their interaction with DMSO. He *et al.* [121] reports that compatibility of PAN/PVA blends calculated through Schneier's theory is complete for concentrations lower than 39% and 87% of PVA content. Outside of this range it is possible that blends have irregular properties what might lead to different freezing temperature and consequently wide pore size distribution.

Table 4.9: Results of properties of hybrid PAN/PVA aerogels at different ratios at concentration 5 wt%.

PVA content (%)	$l_{\text{shrinkage}}$ (%)	Porosity (%)	SSA (m^2g^{-1})
0	14.4 ± 1.2	93.5 ± 0.6	119 ± 18
25	14.4 ± 0.8	93.2 ± 0.5	53 ± 20
50	16.0 ± 1.7	92.8 ± 0.3	55 ± 17
75	17.8 ± 1.9	92.2 ± 0.6	61 ± 30
100	22.4 ± 3.1	90.2 ± 0.8	81 ± 38

Volumetric shrinkage, porosity and specific surface area are shown in average \pm standard deviation. All of the experiments have been repeated at least three times.

In addition, aerogels with 25% PVA content have an specific surface area drastically low although porosity is very similar to pure PAN, 93 ± 1 and $94 \pm 1 \text{ m}^2 \text{ g}^{-1}$. The arrangement of the polymer network concedes DMSO crystals to be bigger in size that lead to pores size outside of the range of BET measurement.

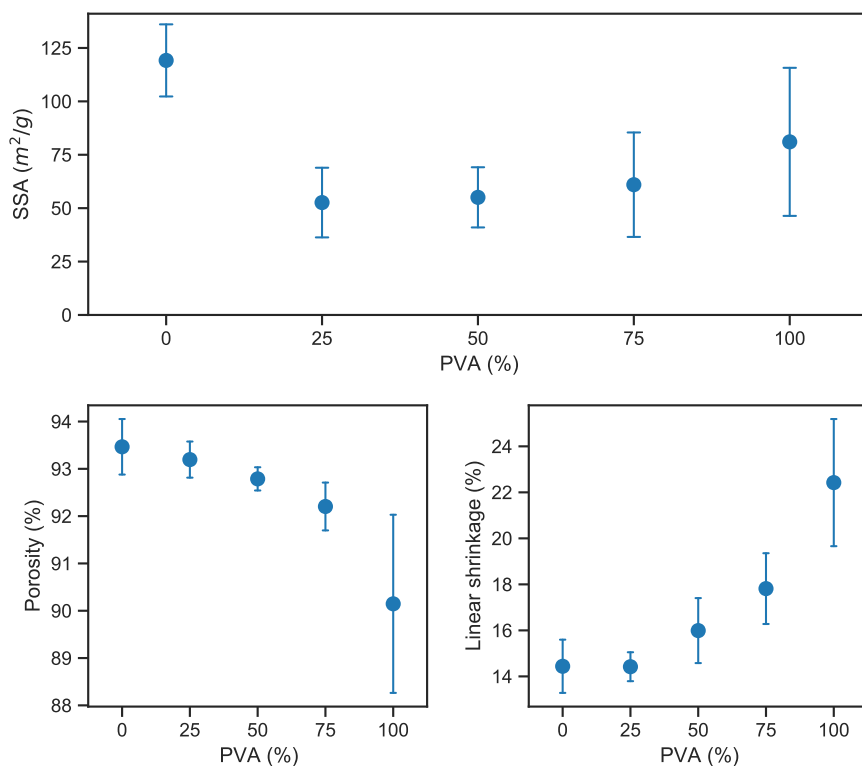


Figure 4.15: Effect of ratio PAN/PVA of aerogels 5 wt % on specific surface area, porosity and linear shrinkage.

4.3.3 PAN/agar-agar aerogels

PAN was combined with agar-agar in order to study the effect of aerogel preparation with two polymers. The results of a solution PAN/agar-agar 50/50% are shown in Table 4.10.

In terms of visual aspect and integrity, throughout the process PAN/agar-agar aerogels are fragile and softer, this condition is specially noticeable after drying where their physical integrity is compromised and some outer parts break into smaller pieces, Figure 4.16. Results of specific surface area, porosity and volumetric shrinkage are shown in Table 4.10

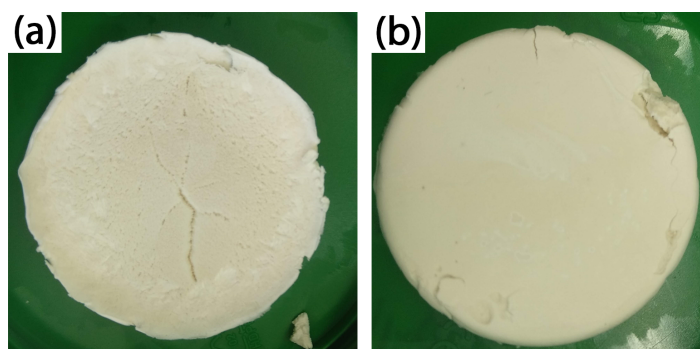


Figure 4.16: PAN/Agar-agar(50/50%) 7.5 wt% aerogel (a) top side (b) bottom side.

Table 4.10: Results of properties of pure PAN and hybrid 50% PAN 50% agar-agar aerogels at different polymer concentration.

Concentration (wt %)	Material	$V_{\text{shrinkage}}$ (%)	Porosity (%)	SSA (m^2g^{-1})
5.0	PAN	36.8 ± 6.1	93.5 ± 0.6	119 ± 18
	PAN/Agar (50/50%)	38.1 ± 2.5	92.4 ± 0.3	6 ± 10
7.5	PAN	41.8 ± 1.3	90.8 ± 0.5	91 ± 15
	PAN/Agar (50/50%)	35.1 ± 2.5	88.7 ± 0.4	6 ± 10

Volumetric shrinkage, porosity and specific surface area are shown in average \pm standard deviation. All of the experiments have been repeated at least three times.

From Figure 4.17 specific surface area lowers drastically. One possible reason could be that the high viscosity of agar-agar in DMSO at those concentrations, leads to large vacancies for the DMSO crystal to grow, hence a prevalence of macropores over mesopores. This explanation is also concordant to porosity values of aerogels at both concentrations similar to pure PAN aerogels. Volumetric shrinkage might suggest that the pore walls formed in PAN/agar solution are thicker than those of only PAN.

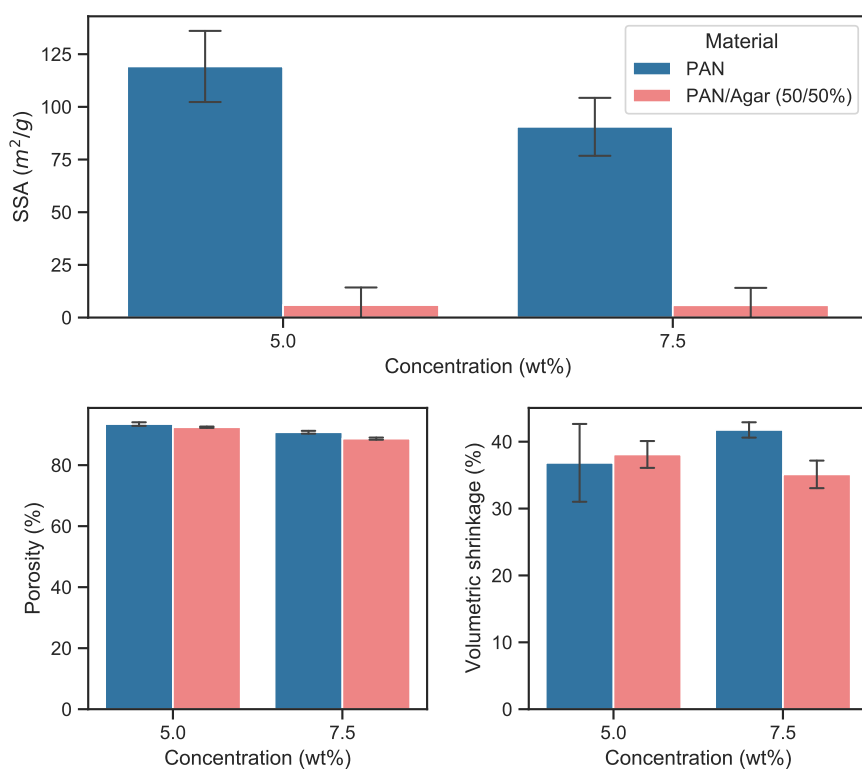


Figure 4.17: Comparison of specific surface area, porosity and volumetric shrinkage of aerogels ■ PAN ■ hybrid PAN/Agar (50/50%).

5. Summary

The aim of this work is to develop and optimize a process for the production of aerogels from precursors (polymers) which usually cannot be used in the conventional aerogel production process due to the lack of the gelling ability. The novel process proceeds via freezing of the precursors' solution in DMSO followed by a cryoextraction step with EtOH and finally by scCO₂ drying of the wet network.

A polymer solution in DMSO is first frozen at $-28\text{ }^{\circ}\text{C}$. Afterwards, frozen monolith undergo a cryoextraction with EtOH at $-28\text{ }^{\circ}\text{C}$. Finally, wet networks are dried in a scCO₂ process at 120 bar and $50\text{ }^{\circ}\text{C}$ for 3 h, resulting in a porous material (aerogel).

Textural properties of the obtained porous materials are characterised by measuring the specific surface area (SSA), porosity (ϵ) and shrinkage (volume reduction throughout the processing). Generally speaking, it is desired to obtain a high specific surface area (over $100\text{ m}^2\text{ g}^{-1}$), along with a high porosity and possibly low shrinkage. Our results show that the polymer concentration in the solution has a strong effect on these properties.

Initial screening is conducted with a series of polymers, phytigel, PAN, PVA, κ -carrageenan, guar flour, pectin, λ -carrageenan, gum arabic, alginic acid, CMC sodium salt (both low and medium viscosity). Among all the polymers, PAN is studied in a more depth due to promising results in comparison to the rest.

To obtain PAN aerogels the polymer concentration is varied between 0.625 and 10 wt %. Concentrations lower than 1.25 wt % results in materials with a high volu-

metric shrinkage, low SSA. Moreover, these materials can easily be electrified. It was found that an optimal concentration for PAN in DMSO lies around 5 wt %. For another polymer, PVA, the optimal concentration is 7.5 wt %. The properties achieved were $\varepsilon = 93.5 \pm 0.6\%$ and $90.6 \pm 3.9\%$ $V_{\text{shrinkage}} = 36.8 \pm 6.1\%$ and $47.7 \pm 5.6\%$ SSA: $119 \pm 18 \text{ m}^2 \text{ g}^{-1}$ and $107 \pm 15 \text{ m}^2 \text{ g}^{-1}$, for PAN and PVA respectively. Based on these results, we can hypothesise that there is an optimal concentration for every polymer.

Freezing rate of the solutions is studied in different ways for PAN solutions. First of all, freezing molds from different materials and of different dimensions were employed. When freezing was performed in a radial direction, the formation of voids in the center of the sample was observed. On the other hand, for freezing in axial direction (from the bottom) the surface presents some discontinuities and a higher shrinkage in the centre than in the outer circle was observed. Hard molds were selected for the easy manipulation of samples, consistent dimension of the mold after multiple experiments and higher specific surface area obtained with them. Moreover, experiments with monoliths with different thicknesses (controlled by the sample weight) reveal that lowering the thickness enhances textural properties, SSA: 119 ± 18 and $53 \pm 20 \text{ m}^2 \text{ g}^{-1}$ for 5 g and 10 g samples respectively. This difference could be attributed to the increase of the freezing rate for samples with lower thickness. Furthermore, the immersion of molds with polymer solution in liquid nitrogen for 2 minutes was tested (so called flash freezing). Aerogels prepared with the flash freezing demonstrate similar volumetric shrinkage and porosity, but the specific surface area is noticeably lower. One possible reason is that being the freezing rate extremely high prevents the diffusion of the polymer creating large DMSO crystals and therefore, bigger pore size. Although these aerogels have a lower SSA, SEM images show no defined pore structure that suggest that frozen glassy state is

reached during freezing.

In addition to aerogels prepared from PAN, hybrid PAN-based aerogels were also studied. Second components tested were urea, PVA and agar-agar. The addition of these additives worsens the quality of the aerogel. When urea is added, large pores are presumably formed since the S_{BET} significantly decreases while porosity increases. We can surmise that the suppression of the formation of hydrogen bonds allows DMSO crystals to grow to bigger sizes resulting in rather macroporous materials with low specific surface area. Combinations of PVA and PAN at 5 wt % reduce the specific area: with increasing the PVA content both porosity and SSA decrease, while the linear shrinkage increases. The addition of agar-agar does not improve properties, and also compromises the sample integrity, resulting aerogels that easily break.

6. Conclusions and outlook

Preparation of PAN aerogels through freezing at $-28\text{ }^{\circ}\text{C}$ followed by cryoextraction with EtOH at $-28\text{ }^{\circ}\text{C}$ and scCO₂ drying at $50\text{ }^{\circ}\text{C}$ and 120 bar is feasible. PAN aerogels at different polymer concentrations have a porosity higher than 85% and the specific surface area higher than $100\text{ m}^2\text{ g}^{-1}$.

Critical aspects of the process that have an impact on the material quality are the polymer concentration and the freezing step. There is an optimal concentration, at which the specific surface area is the highest (all other process variables are kept constant). It was observed that by lowering the polymer concentration higher porosity and SSA can be achieved, but at the same time thinner pore walls are created causing a higher gel shrinkage. Freezing step has a profound effect on the aerogel structure: different freezing conditions (freezing rate, direction) result in different pore structures. Flash freezing in liquid nitrogen yields aerogels with non-hierarchical pore structure that lack physical integrity.

Combination of PAN with PVA or agar creates hybrid aerogels with worse textural properties than those made from PAN only. There is no noticeable trend for the SSA versus the overall polymer concentration for both PAN/PVA and PAN/agar aerogels. Addition of urea to the polymer solution in order to disrupt hydrogen bonds does not improve the aerogel textural properties.

The route via freezing and cryoextraction has been proven to be adequate for the preparation of porous material from PAN. Future research might be conducted to systematically study freezing conditions. The monitoring of the freezing step is cer-

tainly required to gain control over the porous structure and achieve reproducible results. Further research on the phase behaviour of PAN and polymer mixtures in DMSO would help in understand physical state of the system throughout the process and hopefully shed more light on the mechanism of the pore formation.

7. Appendix

Table 7.1: Skeletal densities of polymers.

Polymer	ρ_{skeletal} (g/cm ³)
Alginic acid ammonium salt	1
Xanthan	1.5
CMC Na salt medium viscosity	1.6
CMC Na salt low viscosity	1.6
PAN	1.184 [122]
PVA	1.180 [123]
Inulin	1.35
Gum arabic	1.4
Agar-agar	0.55
k-carrageenan	1.72
Pektin	1.509

7.1 Calibration curves of EtOH and solvent mixtures

The data for the calibration curves is in Table 7.2 and 7.3.

Table 7.2: Density of mixtures of EtOH and DMSO. Calibration data.

DMSO (wt%)	Ethanol (wt%)	1	2	3	Density (g/cm ³)
100	0	1.100	1.100	1.100	1.100
90	10	1.061	1.061	1.061	1.061
80	20	0.991	1.024	1.024	1.013
70	30	0.982	0.983	0.984	0.983
60	40	0.955	0.956	0.954	0.955
50	50	0.922	0.924	0.923	0.923
40	60	0.894	0.897	0.896	0.895
30	70	0.869	0.868	0.871	0.870
20	80	0.839	0.841	0.840	0.840
10	90	0.815	0.816	0.814	0.815
0	100	0.791	0.790	0.790	0.790

Table 7.3: Density of mixtures of EtOH and DMSO aqueous solution of TBA at 20% density. Calibration data.

DMSO (wt%)	TBA/Water (wt%)	1	2	3	Density (g/cm ³)
100	0	0.970	0.971	0.970	0.970
90	10	0.957	0.958	0.957	0.957
80	20	0.939	0.940	0.940	0.940
70	30	0.924	0.925	0.924	0.924
60	40	0.907	0.908	0.908	0.908
50	50	0.889	0.890	0.889	0.889
40	60	0.871	0.872	0.871	0.871
30	70	0.852	0.852	0.852	0.852
20	80	0.832	0.833	0.833	0.833
10	90	0.812	0.813	0.812	0.813
0	100	0.790	0.790	0.790	0.790

Literature

- [1] Philippova, O. and Khokhlov, A. 'Polymer gels'. *Polymer Science: A Comprehensive Reference, 10 Volume Set*. 2012, 339–366.
- [2] Yamauchi, A. 'Gels: introduction'. *Gels handbook*. Elsevier, 2001, 4–12.
- [3] Nayak, A. K. and Das, B. 'Introduction to polymeric gels'. *Polymeric Gels*. Elsevier, 2018, 3–27. DOI: 10.1016/b978-0-08-102179-8.00001-6.
- [4] Fricke, J. and Emmerling, A. Aerogels—Preparation, properties, applications. *Chemistry, Spectroscopy and Applications of Sol-Gel Glasses*. 1992, 37–87.
- [5] Pierre, A. C. 'History of aerogels'. *Aerogels Handbook*. Springer, 2011, 3–18.
- [6] Batista, M. *et al.* Novel alginate-chitosan aerogel fibres for potential wound healing applications. *International journal of biological macromolecules*. 2020.
- [7] Gurikov, P. *et al.* 110th Anniversary: Solvent Exchange in the Processing of Biopolymer Aerogels: Current Status and Open Questions. *Industrial & Engineering Chemistry Research*. 2019, **58**(40), 18590–18600.
- [8] Ching Ma, T. 'Development of novel porous materials by a combination of cryoextraction and supercritical drying technologies'. MA thesis. Hamburg University of Technology, 2020.
- [9] Hägerström, H. 'Polymer gels as pharmaceutical dosage forms: rheological performance and physicochemical interactions at the gel-mucus interface for formulations intended for mucosal drug delivery'. PhD thesis. Acta Universitatis Upsaliensis, 2003.

- [10] Buerkle, L. E. and Rowan, S. J. Supramolecular gels formed from multi-component low molecular weight species. *Chemical Society Reviews*. 2012, **41**(18), 6089–6102.
- [11] Mawad, D., Lauto, A. and Wallace, G. G. 'Conductive polymer hydrogels'. *Polymeric hydrogels as smart biomaterials*. Springer, 2016, 19–44.
- [12] Triboni, E. R. and Moraes, T. B. F. 'Polymeric Gels'. *Nano Design for Smart Gels*. Elsevier, 2019, 71–92.
- [13] Bohidar, H. B., Dubin, P. and Osada, Y. *Polymer gels: fundamentals and applications*. ACS Publications, 2002.
- [14] Osada, Y. 'Section 2 - Polymer gels: Crosslink formations'. *Gels Handbook*. Ed. by Y. Osada *et al.* Burlington: Academic Press, 2001, 13–25. ISBN: 978-0-12-394690-4. DOI: <https://doi.org/10.1016/B978-012394690-4/50076-1>.
- [15] Rogovina, L., Vasil'ev, V. and Braudo, E. Definition of the concept of polymer gel. *Polymer Science Series C*. 2008, **50**(1), 85–92.
- [16] Kavanagh, G. and Ross-Murphy, S. Rheological characterisation of polymer gels. *Progress in Polymer Science*. 1998, **23**, 533–562.
- [17] Khokhlov, A. *Polymer gels and networks*. CRC Press, 2001.
- [18] Bonelli, N. *et al.* 'Confined Aqueous Media for the Cleaning of Cultural Heritage: Innovative Gels and Amphiphile-Based Nanofluids'. *Nanoscience and Cultural Heritage*. Ed. by P. Dillmann, L. Bellot-Gurlet and I. Nenner. Paris: Atlantis Press, 2016, 283–311.
- [19] Wang, W., Narain, R. and Zeng, H. 'Hydrogels'. *Polymer Science and Nanotechnology*. Elsevier, 2020, 203–244.
- [20] Kalia, S. *Polymeric hydrogels as smart biomaterials*. Springer, 2016.

- [21] Ahmed, E. M. Hydrogel: Preparation, characterization, and applications: A review. *Journal of Advanced Research*. 2015, **6**(2), 105–121. ISSN: 2090-1232. DOI: <https://doi.org/10.1016/j.jare.2013.07.006>.
- [22] Ullah, F. *et al.* Classification, processing and application of hydrogels: A review. *Materials Science and Engineering: C*. 2015, **57**, 414–433. ISSN: 0928-4931. DOI: <https://doi.org/10.1016/j.msec.2015.07.053>.
- [23] Majee, S. B. *Emerging concepts in analysis and applications of hydrogels*. BoD–Books on Demand, 2016.
- [24] Ciolacu, D. E. and Suflet, D. M. ‘Cellulose-based hydrogels for medical pharmaceutical applications’. *Biomass as Renewable Raw Material to Obtain Bioproducts of High-Tech Value*. Elsevier, 2018, 401–439.
- [25] Kaczmarek, B., Nadolna, K. and Owczarek, A. ‘The physical and chemical properties of hydrogels based on natural polymers’. *Hydrogels Based on Natural Polymers*. Elsevier, 2020, 151–172.
- [26] Ismail, H., Irani, M. and Ahmad, Z. Starch-based hydrogels: present status and applications. *International Journal of Polymeric Materials and Polymeric Biomaterials*. 2013, **62**(7), 411–420.
- [27] ‘1.3.2E - Hydrogels’. *Biomaterials Science (Fourth Edition)*. Ed. by W. R. Wagner, S. E. Sakiyama-Elbert, G. Zhang and M. J. Yaszemski. Fourth Edition. Academic Press, 2020, 153–166. ISBN: 978-0-12-816137-1.
- [28] Ract, J. N., da Cruz, R. G. and Pereira, C. G. ‘Chapter 14 - Phase Equilibrium of Organogels’. *Thermodynamics of Phase Equilibria in Food Engineering*. Ed. by C. G. Pereira. Academic Press, 2019, 563–591. ISBN: 978-0-12-811556-5. DOI: <https://doi.org/10.1016/B978-0-12-811556-5.00014-4>.

- [29] Vintiloiu, A. and Leroux, J.-C. Organogels and their use in drug delivery—a review. *Journal of controlled release*. 2008, **125**(3), 179–192.
- [30] Esposito, C. L., Kirilov, P. and Roullin, V. G. Organogels, promising drug delivery systems: an update of state-of-the-art and recent applications. *Journal of controlled release*. 2018, **271**, 1–20.
- [31] Sahoo, S. *et al.* Organogels: properties and applications in drug delivery. *Designed monomers and polymers*. 2011, **14**(2), 95–108.
- [32] ‘CHAPTER 1 - Introduction’. *Sol-Gel Science*. Ed. by C. J. Brinker and G. W. Scherer. San Diego: Academic Press, 1990, xvi–18. ISBN: 978-0-08-057103-4. DOI: <https://doi.org/10.1016/B978-0-08-057103-4.50006-4>.
- [33] Scherer, G. ‘Xerogels’. *Encyclopedia of Materials: Science and Technology*. Ed. by K. J. Buschow *et al.* Oxford: Elsevier, 2001, 9797–9799. ISBN: 978-0-08-043152-9. DOI: <https://doi.org/10.1016/B0-08-043152-6/01777-0>.
- [34] Guzel Kaya, G., Yilmaz, E. and Devenci, H. Sustainable nanocomposites of epoxy and silica xerogel synthesized from corn stalk ash: Enhanced thermal and acoustic insulation performance. *Composites Part B: Engineering*. 2018, **150**, 1–6. ISSN: 1359-8368. DOI: <https://doi.org/10.1016/j.compositesb.2018.05.039>.
- [35] Montes, S. and Maleki, H. ‘Aerogels and their applications’. *Colloidal Metal Oxide Nanoparticles*. Elsevier, 2020, 337–399.
- [36] Jackcina Stobel Christy, E., Rajeswari, A., Gopi, S. and Pius, A. ‘Chapter 10 - Chitin and chitosan-based aerogels’. *Handbook of Chitin and Chitosan*. Ed. by S. Gopi, S. Thomas and A. Pius. Elsevier, 2020, 285–334. ISBN: 978-0-12-817970-3. DOI: <https://doi.org/10.1016/B978-0-12-817970-3.00010-9>.

- [37] Zhao, S., Manic, M. S., Ruiz-Gonzalez, F. and Koebel, M. M. Aerogels. *The Sol-Gel Handbook*. 2015, 519–574.
- [38] Şahin, İ. *et al.* Kinetics of supercritical drying of gels. *Gels*. 2018, **4**(1), 3.
- [39] García-González, C., Alnaief, M. and Smirnova, I. Polysaccharide-based aerogels—Promising biodegradable carriers for drug delivery systems. *Carbohydrate Polymers*. 2011, **86**(4), 1425–1438. ISSN: 0144-8617. DOI: <https://doi.org/10.1016/j.carbpol.2011.06.066>.
- [40] Mikhalovsky, S. *et al.* '5.32 - Biomaterials/Cryogels'. *Comprehensive Biotechnology (Third Edition)*. Ed. by M. Moo-Young. Third Edition. Oxford: Pergamon, 2014, 411–423. ISBN: 978-0-444-64047-5. DOI: <https://doi.org/10.1016/B978-0-12-801238-3.04210-0>.
- [41] Plieva, F. M., Galaev, I. Y. and Mattiasson, B. Macroporous gels prepared at subzero temperatures as novel materials for chromatography of particulate-containing fluids and cell culture applications. *Journal of Separation Science*. 2007, **30**(11), 1657–1671. DOI: <https://doi.org/10.1002/jssc.200700127>.
- [42] Microporous membrane formation via thermally-induced phase separation. VI. Effect of diluent morphology and relative crystallization kinetics on polypropylene membrane structure. *Journal of Membrane Science*. 1991, **64**(1), 55–67. ISSN: 0376-7388. DOI: [https://doi.org/10.1016/0376-7388\(91\)80077-J](https://doi.org/10.1016/0376-7388(91)80077-J).
- [43] Zhao, J., Chong, J. Y., Shi, L. and Wang, R. Explorations of combined non-solvent and thermally induced phase separation (N-TIPS) method for fabricating novel PVDF hollow fiber membranes using mixed diluents. *Journal of Membrane Science*. 2019, **572**, 210–222. ISSN: 0376-7388. DOI: <https://doi.org/10.1016/j.memsci.2018.11.015>.

- [44] van de Witte, P., Dijkstra, P., van den Berg, J. and Feijen, J. Phase separation processes in polymer solutions in relation to membrane formation. *Journal of Membrane Science*. 1996, **117**(1), 1–31. ISSN: 0376-7388. DOI: [https://doi.org/10.1016/0376-7388\(96\)00088-9](https://doi.org/10.1016/0376-7388(96)00088-9).
- [45] Tsai, F. J. and Torkelson, J. M. The roles of phase separation mechanism and coarsening in the formation of poly(methyl methacrylate) asymmetric membranes. *Macromolecules*. 1990, **23**(3), 775–784. DOI: 10.1021/ma00205a014.
- [46] Liu, Z., Ran, Y., Xi, J. and Wang, J. Polymeric hybrid aerogels and their biomedical applications. *Soft Matter*. 2020, **16**(40), 9160–9175.
- [47] Nita, L. E. *et al.* New Trends in Bio-Based Aerogels. *Pharmaceutics*. 2020, **12**(5). DOI: 10.3390/pharmaceutics12050449.
- [48] Paraskevopoulou, P., Chriti, D., Raptopoulos, G. and Anyfantis, G. C. Synthetic Polymer Aerogels in Particulate Form. *Materials*. 2019, **12**(9). ISSN: 1996-1944. DOI: 10.3390/ma12091543.
- [49] Sada, K., Kokado, K. and Furukawa, Y. 'Polyacrylonitrile (PAN)'. *Encyclopedia of Polymeric Nanomaterials*. Ed. by S. Kobayashi and K. Müllen. Berlin, Heidelberg: Springer Berlin Heidelberg, 2015, 1745–1750.
- [50] Pan, X., Fantin, M., Yuan, F. and Matyjaszewski, K. Externally controlled atom transfer radical polymerization. *Chemical Society Reviews*. 2018, **47**(14), 5457–5490.
- [51] Selke, S. and Hernandez, R. 'Packaging: Polymers for Containers'. *Encyclopedia of Materials: Science and Technology*. Ed. by K. J. Buschow *et al.* Oxford: Elsevier, 2001, 6646–6652. DOI: <https://doi.org/10.1016/B0-08-043152-6/01175-X>.

- [52] Kausar, A. Polyacrylonitrile-based nanocomposite fibers: A review of current developments. *Journal of Plastic Film & Sheeting*. 2019, **35**(3), 295–316.
- [53] Umemoto, S., Matsumura, T., Sakai, T. and Okui, N. Elongation/contraction properties for poly(acrylonitrile) gel fibers stimulated by pH. *Polymer Gels and Networks*. 1993, **1**(2), 115–126. ISSN: 0966-7822. DOI: [https://doi.org/10.1016/0966-7822\(93\)90015-A](https://doi.org/10.1016/0966-7822(93)90015-A).
- [54] Ramseyer, P. *et al.* In vivo study of an injectable poly(acrylonitrile)-based hydrogel paste as a bulking agent for the treatment of urinary incontinence. *Biomaterials*. 2010, **31**(17), 4613–4619. ISSN: 0142-9612. DOI: <https://doi.org/10.1016/j.biomaterials.2010.02.021>.
- [55] Mao, L. *et al.* Structure and character of artificial muscle model constructed from fibrous hydrogel. English. *Current Applied Physics*. 2005, **5**(5), 426–428. DOI: [10.1016/j.cap.2004.11.003](https://doi.org/10.1016/j.cap.2004.11.003).
- [56] Yu, L. and Gu, L. Effects of microstructure, crosslinking density, temperature and exterior load on dynamic pH-response of hydrolyzed polyacrylonitrile-blend-gelatin hydrogel fibers. *European Polymer Journal*. 2009, **45**(6), 1706–1715. ISSN: 0014-3057. DOI: <https://doi.org/10.1016/j.eurpolymj.2009.03.002>.
- [57] Aoki, K., Haniu, H., Kim, Y. A. and Saito, N. The Use of Electrospun Organic and Carbon Nanofibers in Bone Regeneration. *Nanomaterials*. 2020, **10**(3). ISSN: 2079-4991. DOI: [10.3390/nano10030562](https://doi.org/10.3390/nano10030562).
- [58] Abd El-Aziz, A. *et al.* Preparation and characterization of carbon nanofibrous/hydroxyapatite sheets for bone tissue engineering. *Materials Science and Engineering: C*. 2017, **76**, 1188–1195. ISSN: 0928-4931. DOI: <https://doi.org/10.1016/j.msec.2017.02.053>.

- [59] Bhuiyan, M. R. *et al.* Electrospun polyacrylonitrile–silica aerogel coating on viscose nonwoven fabric for versatile protection and thermal comfort. *Cellulose*. 2020, **27**(17), 10501–10517.
- [60] Arakawa, C. K. and DeForest, C. A. 'Chapter 19 - Polymer Design and Development'. *Biology and Engineering of Stem Cell Niches*. Ed. by A. Vishwakarma and J. M. Karp. Boston: Academic Press, 2017, 295–314. ISBN: 978-0-12-802734-9. DOI: <https://doi.org/10.1016/B978-0-12-802734-9.00019-6>.
- [61] Li, D. ('5 - Choice of materials for cut protective textile'. *Cut Protective Textiles*. Ed. by D. (Li. The Textile Institute Book Series. Woodhead Publishing, 2020, 129–218. DOI: <https://doi.org/10.1016/B978-0-12-820039-1.00005-5>.
- [62] Satoh, K. 'Poly(vinyl alcohol) (PVA)'. *Encyclopedia of Polymeric Nanomaterials*. Springer Berlin Heidelberg, 2014, 1–6. DOI: 10.1007/978-3-642-36199-9_246-1.
- [63] Alonso-Mougán, M. *et al.* Rheological behaviour of an amide pectin. *Journal of Food Engineering*. 2002, **55**(2), 123–129. ISSN: 0260-8774. DOI: [https://doi.org/10.1016/S0260-8774\(02\)00026-2](https://doi.org/10.1016/S0260-8774(02)00026-2).
- [64] Chen, J. *et al.* Amino acid-amidated pectin: Preparation and characterization. *Food Chemistry*. 2020, **309**, 125768. ISSN: 0308-8146. DOI: <https://doi.org/10.1016/j.foodchem.2019.125768>.
- [65] Reitsma, J., Thibault, J. and Pilnik, W. Properties of amidated pectins. I. Preparation and characterization of amidated pectins and amidated pectic acids. *Food Hydrocolloids*. 1986, **1**(2), 121–127. ISSN: 0268-005X. DOI: [https://doi.org/10.1016/S0268-005X\(86\)80014-5](https://doi.org/10.1016/S0268-005X(86)80014-5).
- [66] Sinitsya, A. *et al.* Amidation of highly methoxylated citrus pectin with primary amines. *Carbohydrate polymers*. 2000, **42**(4), 359–368.

- [67] BeMiller, J. N. '8 - Cellulose and Cellulose-Based Hydrocolloids'. *Carbohydrate Chemistry for Food Scientists (Third Edition)*. Third Edition. AACC International Press, 2019, 223–240. ISBN: 978-0-12-812069-9. DOI: <https://doi.org/10.1016/B978-0-12-812069-9.00008-X>.
- [68] 'Sodium Carboxymethylcellulose'. *Cellulose and Cellulose Derivatives in the Food Industry*. John Wiley & Sons, Ltd, 2014. Chap. 10, 387–478. DOI: <https://doi.org/10.1002/9783527682935.ch10>.
- [69] Yang, X. H. and Zhu, W. L. Viscosity properties of sodium carboxymethylcellulose solutions. *Cellulose*. 2007, **14**(5), 409–417.
- [70] Benchabane, A. and Bekkour, K. Rheological properties of carboxymethyl cellulose (CMC) solutions. *Colloid and Polymer Science*. 2008, **286**(10), 1173.
- [71] Ibrahim, A. A., Adel, A. M., Abd El-Wahab, Z. H. and Al-Shemy, M. T. Utilization of carboxymethyl cellulose based on bean hulls as chelating agent. Synthesis, characterization and biological activity. *Carbohydrate polymers*. 2011, **83**(1), 94–115.
- [72] Anderson-Dekkers, I., Nouwens-Roest, M., Peters, B. and Vaughan, E. 'Chapter 17 - Inulin'. *Handbook of Hydrocolloids (Third Edition)*. Ed. by G. O. Phillips and P. A. Williams. Third Edition. Woodhead Publishing, 2021, 537–562. ISBN: 978-0-12-820104-6. DOI: <https://doi.org/10.1016/B978-0-12-820104-6.00015-2>.
- [73] Silva, R. Use of inulin as a natural texture modifier. *Cereal Foods World*. 1996, **41**(10), 792–794.
- [74] Shoaib, M. *et al.* Inulin: Properties, health benefits and food applications. *Carbohydrate polymers*. 2016, **147**, 444–454.

- [75] Verdonk, J., Shim, S., Van Leeuwen, P. and Verstegen, M. Application of inulin-type fructans in animal feed and pet food. *British Journal of Nutrition*. 2005, **93**(S1), S125–S138.
- [76] Williams, P. A. and Phillips, G. O. 'Chapter 21 - Gum arabic'. *Handbook of Hydrocolloids (Third Edition)*. Ed. by G. O. Phillips and P. A. Williams. Third Edition. Woodhead Publishing, 2021, 627–652. ISBN: 978-0-12-820104-6. DOI: <https://doi.org/10.1016/B978-0-12-820104-6.00022-X>.
- [77] BeMiller, J. N. '16 - Gum Arabic and Other Exudate Gums'. *Carbohydrate Chemistry for Food Scientists (Third Edition)*. Ed. by J. N. BeMiller. Third Edition. AACC International Press, 2019, 313–321. ISBN: 978-0-12-812069-9. DOI: <https://doi.org/10.1016/B978-0-12-812069-9.00016-9>.
- [78] Dauqan, E. and Abdullah, A. Utilization of gum arabic for industries and human health. *American Journal of Applied Sciences*. 2013, **10**(10), 1270.
- [79] Praiboon, J. *et al.* Physical and chemical characterization of agar polysaccharides extracted from the Thai and Japanese species of Gracilaria. *Science Asia*. 2006, **32**(1), 11–17.
- [80] Science of Cooking. *Chemical and Physical Properties of Agar in Cooking*. 15th Mar. 2021. Available at: https://www.scienceofcooking.com/chemical_physical_properties_agar.htm.
- [81] '9.08 - Polysaccharides'. *Polymer Science: A Comprehensive Reference*. Ed. by K. Matyjaszewski and M. Möller. Amsterdam: Elsevier, 2012, 137–155. ISBN: 978-0-08-087862-1. DOI: <https://doi.org/10.1016/B978-0-444-53349-4.00246-6>.

- [82] Armisén, R. and Gaiatas, F. '4 - Agar'. *Handbook of Hydrocolloids (Second Edition)*. Ed. by G. Phillips and P. Williams. Second Edition. Woodhead Publishing Series in Food Science, Technology and Nutrition. Woodhead Publishing, 2009, 82–107. ISBN: 978-1-84569-414-2. DOI: <https://doi.org/10.1533/9781845695873.82>.
- [83] Shamsuri, A., Abdullah, D. and Daik, R. Fabrication of agar/biopolymer blend aerogels in ionic liquid and co-solvent mixture. *Cellulose Chemistry and Technology*. Jan. 2012, **46**, 45–52.
- [84] Chen, L. *et al.* High performance agar/graphene oxide composite aerogel for methylene blue removal. *Carbohydrate Polymers*. 2017, **155**. cited By 145, 345–353. DOI: 10.1016/j.carbpol.2016.08.047.
- [85] Zhang, W. *et al.* Agar aerogel containing small-sized zeolitic imidazolate framework loaded carbon nitride: a solar-triggered regenerable decontaminant for convenient and enhanced water purification. *ACS Sustainable Chemistry & Engineering*. 2017, **5**(10), 9347–9354.
- [86] Cardea, S., Pisanti, P. and Reverchon, E. Generation of chitosan nanoporous structures for tissue engineering applications using a supercritical fluid assisted process. *The Journal of Supercritical Fluids*. 2010, **54**(3). Special Issue - Supercritical Fluid Processing of Biopolymers and Biomaterials, 290–295. ISSN: 0896-8446. DOI: <https://doi.org/10.1016/j.supflu.2010.05.014>.
- [87] Cardea, S. *et al.* Supercritical gel drying: A powerful tool for tailoring symmetric porous pvdf- hfp membranes. *ACS applied materials & interfaces*. 2009, **1**(1), 171–180.
- [88] Li, Y. *et al.* Nanocellulose aerogels inspired by frozen tofu. *ACS Sustainable Chemistry & Engineering*. 2017, **5**(8), 6387–6391.

- [89] Jin, H., Nishiyama, Y., Wada, M. and Kuga, S. Nanofibrillar cellulose aerogels. *Colloids and Surfaces A: Physicochemical and Engineering Aspects*. 2004, **240**(1), 63–67. ISSN: 0927-7757. DOI: <https://doi.org/10.1016/j.colsurfa.2004.03.007>.
- [90] Ishida, O. *et al.* Microfibrillar carbon from native cellulose. *Cellulose*. 2004, **11**(3), 475–480.
- [91] Lozinsky, V. I. *et al.* Cryostructuring of polymer systems. 47. Preparation of wide porous gelatin-based cryostructurates in sterilizing organic media and assessment of the suitability of thus formed matrices as spongy scaffolds for 3D cell culturing. *e-Polymers*. 2018, **18**(2), 175–186. DOI: [doi:10.1515/epoly-2017-0151](https://doi.org/10.1515/epoly-2017-0151).
- [92] Borisova, A. *et al.* A sustainable freeze-drying route to porous polysaccharides with tailored hierarchical meso-and macroporosity. *Macromolecular rapid communications*. 2015, **36**(8), 774–779.
- [93] Yanagisawa, K., Harada, M. and Okada, T. Liquid–Liquid Extraction from Frozen Aqueous Phases Enhances Efficiency with Reduced Volumes of Organic Solvent. *ACS Sustainable Chemistry & Engineering*. 2018, **6**(8), 10120–10126.
- [94] Morales-Román, R. M. *et al.* Freeze-extraction microporous electroactive supports for cell culture. *European Polymer Journal*. 2019, **119**, 531–540. ISSN: 0014-3057. DOI: <https://doi.org/10.1016/j.eurpolymj.2019.07.011>.
- [95] Rutter, J. and Chalmers, B. A prismatic substructure formed during solidification of metals. *Canadian Journal of Physics*. 1953, **31**(1), 15–39.

- [96] Voges, K., Hübner, C., Vadalá, M. and Lupascu, D. C. Ice-Templated Poly (vinyl alcohol): Enhanced Strength and Low Thermal Conductivity. *Macromolecular Materials and Engineering*. 2018, **303**(9), 1800198.
- [97] Zhang, Q. *et al.* Wood-inspired fabrication of polyacrylonitrile solid foam with superfast and high absorption capacity for liquid without selectivity. *ACS applied materials & interfaces*. 2018, **10**(49), 41871–41877.
- [98] Maleki, H. *et al.* Synthesis and biomedical applications of aerogels: Possibilities and challenges. *Advances in Colloid and Interface Science*. 2016, **236**, 1–27. ISSN: 0001-8686. DOI: <https://doi.org/10.1016/j.cis.2016.05.011>.
- [99] Subrahmanyam, R. *et al.* On the road to biopolymer aerogels—Dealing with the solvent. *Gels*. 2015, **1**(2), 291–313.
- [100] Santos, N. C., Figueira-Coelho, J., Martins-Silva, J. and Saldanha, C. Multidisciplinary utilization of dimethyl sulfoxide: pharmacological, cellular, and molecular aspects. *Biochemical Pharmacology*. 2003, **65**(7), 1035–1041. ISSN: 0006-2952. DOI: [https://doi.org/10.1016/S0006-2952\(03\)00002-9](https://doi.org/10.1016/S0006-2952(03)00002-9).
- [101] NIST Chemistry WebBook. *Dimethyl Sulfoxide*. 10th Feb. 2021. Available at: <https://webbook.nist.gov/cgi/cbook.cgi?ID=C67685&Mask=4#ref-2>.
- [102] Iovleva, M., Smirnova, V. and Budnitskii, G. The solubility of polyacrylonitrile. *Fibre Chemistry*. 2001, **33**(4), 262–264.
- [103] Hattori, M. *et al.* NMR study on the dissolved state of polyacrylonitrile in various solvents. *Polymer journal*. 1996, **28**(7), 594–600.
- [104] Wong, D. and Parasrampur, J. 'Polyvinyl Alcohol'. Ed. by H. G. Brittain. Vol. 24. Analytical Profiles of Drug Substances and Excipients. Academic Press, 1996, 397–441. DOI: [https://doi.org/10.1016/S0099-5428\(08\)60699-1](https://doi.org/10.1016/S0099-5428(08)60699-1).

- [105] Mensink, M. A., Frijlink, H. W., van der Voort Maarschalk, K. and Hinrichs, W. L. Inulin, a flexible oligosaccharide I: Review of its physicochemical characteristics. *Carbohydrate Polymers*. 2015, **130**, 405–419. ISSN: 0144-8617. DOI: <https://doi.org/10.1016/j.carbpol.2015.05.026>.
- [106] Dogenski, M. *et al.* Starch-Based Aerogels Obtained via Solvent-Induced Gelation. *Gels*. 2020, **6**(3). ISSN: 2310-2861. Available at: <https://www.mdpi.com/2310-2861/6/3/32>.
- [107] Brunauer, S., Emmett, P. H. and Teller, E. Adsorption of Gases in Multimolecular Layers. *Journal of the American Chemical Society*. 1938, **60**(2), 309–319. DOI: 10.1021/ja01269a023.
- [108] Shaji, A. and Zachariah, A. K. 'Chapter 9 - Surface Area Analysis of Nanomaterials'. *Thermal and Rheological Measurement Techniques for Nanomaterials Characterization*. Ed. by S. Thomas, R. Thomas, A. K. Zachariah and R. K. Mishra. Micro and Nano Technologies. Elsevier, 2017, 197–231. ISBN: 978-0-323-46139-9. DOI: <https://doi.org/10.1016/B978-0-323-46139-9.00009-8>.
- [109] Sing, K. S., Rouquerol, F. and Rouquerol, J. '5 - Classical Interpretation of Physisorption Isotherms at the Gas–Solid Interface'. *Adsorption by Powders and Porous Solids (Second Edition)*. Ed. by F. Rouquerol *et al.* Second Edition. Oxford: Academic Press, 2014, 159–189. ISBN: 978-0-08-097035-6. DOI: <https://doi.org/10.1016/B978-0-08-097035-6.00005-X>.
- [110] Everett, D. H., Parfitt, G. D., Sing, K. S. W. and Wilson, R. The SCI/IUPAC/NPL project on surface area standards. *Journal of Applied Chemistry and Biotechnology*. 1974, **24**(4-5), 199–219. DOI: <https://doi.org/10.1002/jctb.2720240404>.
- [111] Davis, B. H. 'The BET Equation – Nominated for a Nobel Prize but Not Selected'. *The Posthumous Nobel Prize in Chemistry. Volume 1. Correcting the Er-*

- rors and Oversights of the Nobel Prize Committee*. 2017. Chap. 8, 165–206. DOI: 10.1021/bk-2017-1262.ch008.
- [112] Zhou, W., Apkarian, R., Wang, Z. L. and Joy, D. ‘Fundamentals of scanning electron microscopy (SEM)’. *Scanning microscopy for nanotechnology*. Springer, 2006, 1–40.
- [113] Inkson, B. ‘2 - Scanning electron microscopy (SEM) and transmission electron microscopy (TEM) for materials characterization’. *Materials Characterization Using Nondestructive Evaluation (NDE) Methods*. Ed. by G. Hübschen, I. Altpeter, R. Tschuncky and H.-G. Herrmann. Woodhead Publishing, 2016, 17–43. ISBN: 978-0-08-100040-3. DOI: <https://doi.org/10.1016/B978-0-08-100040-3.00002-X>.
- [114] Robitzer, M. *et al.* Nanostructure of Calcium Alginate Aerogels Obtained from Multistep Solvent Exchange Route. *Langmuir*. 2008, **24**(21), 12547–12552. DOI: 10.1021/la802103t.
- [115] Takeshita, S. *et al.* Formation of nanofibrous structure in biopolymer aerogel during supercritical CO₂ processing: The case of chitosan aerogel. *Biomacromolecules*. 2019, **20**(5), 2051–2057.
- [116] Gutiérrez, M. C. *et al.* Poly(vinyl alcohol) Scaffolds with Tailored Morphologies for Drug Delivery and Controlled Release. *Advanced Functional Materials*. 2007, **17**(17), 3505–3513. DOI: <https://doi.org/10.1002/adfm.200700093>.
- [117] Aubert, J. and Clough, R. Low-density, microcellular polystyrene foams. *Polymer*. 1985, **26**(13), 2047–2054. ISSN: 0032-3861. DOI: [https://doi.org/10.1016/0032-3861\(85\)90186-7](https://doi.org/10.1016/0032-3861(85)90186-7).

- [118] Gun'ko, V. M., Savina, I. N. and Mikhalovsky, S. V. Cryogels: Morphological, structural and adsorption characterisation. *Advances in Colloid and Interface Science*. 2013, **187-188**, 1–46. ISSN: 0001-8686. DOI: <https://doi.org/10.1016/j.cis.2012.11.001>.
- [119] Wang, B., Ji, J. and Li, K. Crystal nuclei templated nanostructured membranes prepared by solvent crystallization and polymer migration. *Nature communications*. 2016, **7(1)**, 1–8.
- [120] Sivadevi, S. *et al.* Proton-conducting polymer electrolyte based on PVA-PAN blend doped with ammonium thiocyanate. *Ionics*. 2015, **21(4)**, 1017–1029.
- [121] He, C. *et al.* Blending based polyacrylonitrile/poly(vinyl alcohol) membrane for rechargeable lithium ion batteries. *Journal of Membrane Science*. 2018, **560**, 30–37. ISSN: 0376-7388. DOI: <https://doi.org/10.1016/j.memsci.2018.05.013>.
- [122] Wypych, G. 'PAN polyacrylonitrile'. *Handbook of Polymers*. Ed. by G. Wypych. Oxford: Elsevier, 2012, 264–268. ISBN: 978-1-895198-47-8. DOI: <https://doi.org/10.1016/B978-1-895198-47-8.50084-9>.
- [123] PubChem. *Polyvinyl alcohol*. 20th Feb. 2021. Available at: <https://pubchem.ncbi.nlm.nih.gov/compound/Polyvinyl-alcohol>.